JOURNAL OF GEOPHYSICAL RESEARCH, VOL. 108, NO. B6, 2311, doi:10.1029/2002JB002290, 2003

Inversion of Earth's changing shape to weigh sea level in static equilibrium with surface mass redistribution

Geoffrey Blewitt[1]
Nevada Bureau of Mines and Geology and Seismological Laboratory, University of Nevada, Reno, Nevada, USA

Peter Clarke
School of Civil Engineering and Geosciences, University of Newcastle, Newcastle upon Tyne, UK

Received 4 November 2002; revised 6 February 2003; accepted 5 March 2003; published 21 June 2003.

[1] We develop a spectral inversion method for mass redistribution on the Earth's surface given geodetic measurements of the solid Earth's geometrical shape, using the elastic load Love numbers. First, spectral coefficients are geodetically estimated to some degree. Spatial inversion then finds the continental surface mass distribution that would force geographic variations in relative sea level such that it is self-consistent with an equipotential top surface and the deformed ocean bottom surface and such that the total (ocean plus continental mass) load has the same estimated spectral coefficients. Applying this theory, we calculate the contribution of seasonal interhemispheric (degree 1) mass transfer to variation in global mean sea level and nonsteric static ocean topography, using published GPS results for seasonal degree-1 surface loading from the global IGS network. Our inversion yields ocean-continent mass exchange with annual amplitude $(2.92 \pm 0.14) \times 10^{15}$ kg and maximum ocean mass on 25 August ±3 days. After correction for the annual variation in global mean vertical deformation of the ocean floor (0.4 mm amplitude), we find geocentric sea level has an amplitude of 7.6 ± 0.4 mm, consistent with TOPEX-Poseidon results (minus steric effects). The seasonal variation in sea level at a point strongly depends on location ranging from 3 to 19 mm, the largest being around Antarctica in mid-August. Seasonal gradients in static topography have amplitudes of up to 10 mm over 5000 km, which may be misinterpreted as dynamic topography. Peak continental loads occur at high latitudes in late winter at the water-equivalent level of 100–200 mm. *INDEX TERMS:* 1214 Geodesy and Gravity: Geopotential theory and determination; 1223 Geodesy and Gravity: Ocean/Earth/atmosphere interactions (3339); 1655 Global Change: Water cycles (1836); 4203 Oceanography: General: Analytical modeling; 4227 Oceanography: General: Diurnal, seasonal, and annual cycles; *KEYWORDS:* Earth's shape, mass redistribution, GPS, Love number, geoid, sea level

Citation: Blewitt, G., and P. Clarke, Inversion of Earth's changing shape to weigh sea level in static equilibrium with surface mass redistribution, *J. Geophys. Res.*, *108*(B6), 2311, doi:10.1029/2002JB002290, 2003.

1. Introduction

[2] We develop a methodology to invert for the redistribution of fluids on the Earth's surface given precise global geodetic measurements of Earth's geometrical shape. Specifically we develop (1) inversion of geodetic station coordinates for a spherical harmonic representation of Earth's shape; (2) inversion of Earth's shape for surface mass distribution; (3) inversion for a specific surface mass distribution consistent with static equilibrium theory on the ocean's passive response to mass redistribution on land. Finally, we demonstrate the developed methodology in the simplest possible case, using a published empirical seasonal model of degree-1 coefficients, and we assess the feasibility of higher resolution inversion. Figure 1 presents an overview of the overall scheme, where here the focus is on inversion for the surface load using station positions.

[3] This development is motivated by recent advances in monitoring the changing shape of the Earth. For example, consider the global polyhedron formed by the current ~250 Global Positioning System (GPS) stations of the International GPS Service. A time series of estimated polyhedra can be estimated every week [*Davies and Blewitt*, 2000], which can then be converted into low-degree spherical harmonic coefficients describing the shape of the Earth as a function of time [*Blewitt et al.*, 2001]. Earlier work by *Plag et al.* [1996] suggested the possibility of using space geodetic measurements together with a "known" surface

[1]Also at School of Civil Engineering and Geosciences, University of Newcastle, Newcastle upon Tyne, UK.

0148-0227/03/2002JB002290$09.00

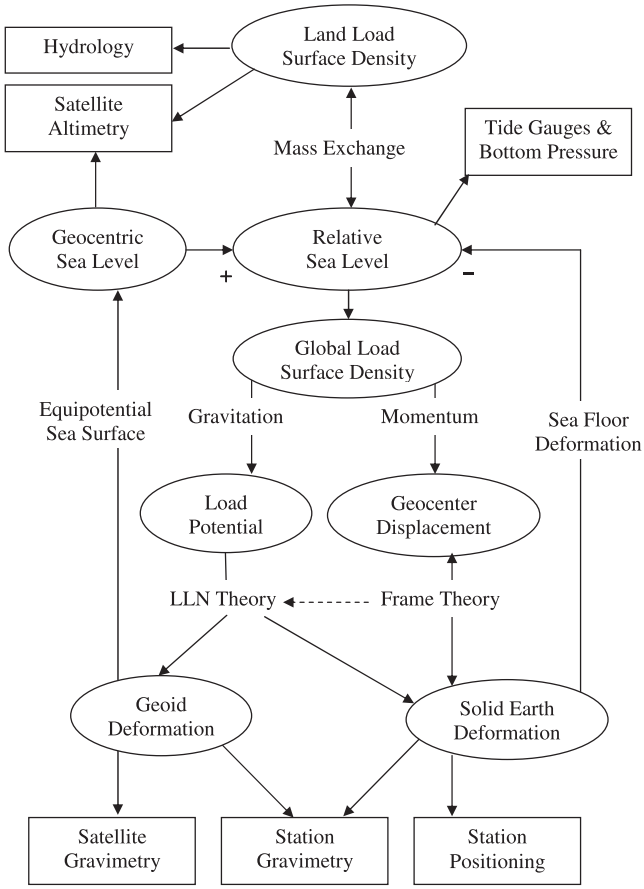

Figure 1. The basic elements of our analytical integrated loading model, building on a figure from *Blewitt* [2003], which incorporated self-consistency of the reference frame and loading dynamics. Here we incorporate self-consistency in the static, passive response of ocean loading. Phenomena are in ovals, measurement types are in rectangles, and physical principles are attached to the connecting arrows. The arrows indicate the direction leading toward the computation of measurement models, which this paper inverts for the case of measured station positions. Although the diagram suggests an iterative forward modeling solution [e.g., *Wahr*, 1982], we develop a closed-form solution that allows for true inversion.

mass distribution to then invert for Earth's mechanical properties. However, more recent evidence suggests that uncertainties in the surface load distribution are generally far more significant than differences between Earth mechanical models [*van Dam et al.*, 1997, 2001; *Tamisiea et al.*, 2002]. Hence the focus of this paper is the opposite problem, that is, the estimation of consistent load distributions, given known mechanical properties of the Earth. Using the theory developed here, we can in effect use geodetic measurements of land deformation to "weigh" separately the loading of continental water and the passive response of sea level. The method also produces estimates of variations in the geoid height and the ocean's static topography, which have application to the interpretation of satellite altimeter data in terms of the ocean's dynamic topography. Expressions are also obtained to estimate change in global mean sea level and the mass of water exchanged between the oceans and the continents.

[4] We apply the following development to elastic loading theory and equilibrium tidal theory for the investigation of mass redistribution over timescales of weeks to decades. At shorter time periods, ocean currents and tidal friction play a dominant role; at longer time periods, mantle viscosity effects start to dominate. As elastic loading is the only deformation process considered here, it is implicitly assumed that geodetic coordinates have been calibrated for other types of solid Earth deformations of such as lunisolar tidal deformation, secular motion due to plate tectonics and postglacial rebound, and transient motions due to the earthquake cycle. It is also extremely important to calibrate for GPS station configuration changes, especially antennas.

2. Spectral Inversion for Earth's Changing Shape

[5] Consider a network of geodetic stations located at geographical positions Ω_i (latitude φ_i, longitude λ_i for $i = 1,\ldots,s$) that provide a time series of station coordinate displacements ($e_i n_i u_i$), corresponding to local east, north, and up in a global terrestrial reference frame [*Davies and Blewitt*, 2000]. As a first step, we develop a purely kinematic model of these vector displacements as a spectral expansion of appropriate basis functions over the Earth's surface, independent of specific loading models. This leads to expressions for least squares estimates of the empirical spectral parameters. This step is therefore independent of the dynamics responsible for the deformation (except for consideration of appropriate spatial resolution).

2.1. Kinematic Spectral Displacement Model

[6] Consider a vector surface displacement function on a sphere decomposed into lateral and height components:

$$\mathbf{D}(\Omega) = E(\Omega)\hat{\boldsymbol{\lambda}} + N(\Omega)\hat{\boldsymbol{\varphi}} + H(\Omega)\hat{\mathbf{r}} \tag{1}$$

where $(\hat{\boldsymbol{\lambda}}, \hat{\boldsymbol{\varphi}}, \hat{\mathbf{r}})$ are unit vectors forming a right-handed topocentric coordinate basis pointing respectively in directions east, north, and up. It can be shown [*Grafarend*, 1986] that the lateral component of the displacement function can also be decomposed into poloidal (or "spheroidal") and toroidal components, so we can write

$$\mathbf{D}(\Omega) = \nabla\Psi(\Omega) + \nabla \times (\Gamma(\Omega)\hat{\mathbf{r}}) + H(\Omega)\hat{\mathbf{r}} \tag{2}$$

where $\Psi(\Omega)$ is the scalar poloidal surface function, $\Gamma(\Omega)$ is the scalar toroidal surface function, and the surface gradient operator is defined by

$$\nabla = \hat{\boldsymbol{\lambda}}(1/\cos\varphi)\partial_\lambda + \hat{\boldsymbol{\varphi}}\partial_\varphi \tag{3}$$

Invoking the Love-Shida hypothesis [*Love*, 1909] that no toroidal displacements are forced by surface-normal loading, so $\Gamma(\Omega) = 0$, we can express the east and north functions in terms of the poloidal component:

$$\begin{aligned} E(\Omega) &= (1/\cos\varphi)\partial_\lambda\Psi(\Omega) \\ N(\Omega) &= \partial_\varphi\Psi(\Omega) \end{aligned} \tag{4}$$

Let us model the height and poloidal functions as spherical harmonic expansions truncated to degree $\bar{n}$:

$$H(\Omega) = \sum_{n=1}^{\bar{n}} \sum_{m=0}^{n} \sum_{\Phi}^{\{C,S\}} H_{nm}^{\Phi} Y_{nm}^{\Phi}(\Omega)$$
$$\Psi(\Omega) = \sum_{n=1}^{\bar{n}} \sum_{m=0}^{n} \sum_{\Phi}^{\{C,S\}} \Psi_{nm}^{\Phi} Y_{nm}^{\Phi}(\Omega) \tag{5}$$

where our spherical harmonics convention is given in Appendix A and truncation issues are discussed later. We define the summation over $\Phi \in \{C, S\}$ where C and S identify sine and cosine components of the expansion. From equations (4) and (5), the east and north functions are therefore modeled by [*Grafarend*, 1986, p. 340]

$$E(\Omega) = \sum_{n=1}^{\bar{n}} \sum_{m=0}^{n} \sum_{\Phi}^{\{C,S\}} \Psi_{nm}^{\Phi} \frac{\partial_{\lambda} Y_{nm}^{\Phi}(\Omega)}{\cos\varphi}$$
$$N(\Omega) = \sum_{n=1}^{\bar{n}} \sum_{m=0}^{n} \sum_{\Phi}^{\{C,S\}} \Psi_{nm}^{\Phi} \partial_{\varphi} Y_{nm}^{\Phi}(\Omega) \tag{6}$$

2.2. Degree-0 Considerations

[7] The summation for the height function begins at $n = 1$ because a nonzero $H_{00}^{C} Y_{00}^{C}$ implies an average change in the Earth's radius, which is theoretically forbidden in a spherically symmetric Earth model where the total surface mass is constant. The summation for the poloidal function begins at $n = 1$ simply because $Y_{00}^{C} = 1$ and therefore its surface gradient is zero. Hence the degree-0 coefficient is arbitrary as it cannot affect the lateral velocity field. We choose to fix the gauge of the scalar field $\Psi(\Omega)$ by setting $\Psi_{00}^{C} = 0$.

2.3. Degree-1 Considerations

[8] The degree-1 component of displacement is a subtle problem [*Farrell*, 1972; *Blewitt*, 2003] and should not mistakenly be represented as a pure translation. Furthermore, we must carefully consider degree-1 deformation because there are only three (not six) independent components of the displacement field. Let us start by writing the degree-1 component of the vector displacement as a function of the six degree-1 parameters from equations (1), (5), and (6):

$$\begin{aligned}
&\mathbf{D}_1(\Omega) \\
&= \sum_{m=0}^{1} \sum_{\Phi}^{\{C,S\}} \left(\hat{\boldsymbol{\lambda}} \Psi_{1m}^{\Phi} \frac{\partial_{\lambda} Y_{1m}^{\Phi}(\Omega)}{\cos\varphi} + \hat{\boldsymbol{\varphi}} \Psi_{1m}^{\Phi} \partial_{\varphi} Y_{1m}^{\Phi}(\Omega) + \hat{\mathbf{r}} H_{1m}^{\Phi} Y_{1m}^{\Phi}(\Omega) \right) \\
&= \hat{\boldsymbol{\lambda}} \left(-\Psi_{11}^{C} \sin\lambda + \Psi_{11}^{S} \cos\lambda \right) \\
&+ \hat{\boldsymbol{\varphi}} \left(-\Psi_{11}^{C} \sin\varphi\cos\lambda - \Psi_{11}^{S} \sin\varphi\sin\lambda + \Psi_{10}^{C} \cos\varphi \right) \\
&+ \hat{\mathbf{r}} \left(H_{11}^{C} \cos\varphi\cos\lambda + H_{11}^{S} \cos\varphi\sin\lambda + H_{10}^{C} \sin\varphi \right)
\end{aligned} \tag{7}$$

This is equivalent to the vector formula:

$$\mathbf{D}_1(\Omega) = \hat{\boldsymbol{\lambda}} \left(\boldsymbol{\Psi}_1 . \hat{\boldsymbol{\lambda}} \right) + \hat{\boldsymbol{\varphi}} (\boldsymbol{\Psi}_1 . \hat{\boldsymbol{\varphi}}) + \hat{\mathbf{r}} (\mathbf{H}_1 . \hat{\mathbf{r}}) = \boldsymbol{\Psi}_1 + \hat{\mathbf{r}} [(\mathbf{H}_1 - \boldsymbol{\Psi}_1) . \hat{\mathbf{r}}] \tag{8}$$

where we define the spatially constant vectors $\boldsymbol{\Psi}_1 = (\Psi_{11}^{C}, \Psi_{11}^{S}, \Psi_{10}^{C})$ and $\mathbf{H}_1 = (H_{11}^{C}, H_{11}^{S}, \mathrm{H}_{10}^{C})$. The same degree-1 deformation, as observed in a reference frame that has an origin displaced by vector $\Delta\mathbf{r} = (\Delta x, \Delta y, \Delta z)$ with respect to the original frame, will have surface displacements (denoted with primes)

$$\mathbf{D}'_1(\Omega) = \mathbf{D}_1(\Omega) - \Delta\mathbf{r} = \boldsymbol{\Psi}'_1 + \hat{\mathbf{r}} \left[\left(\mathbf{H}'_1 - \boldsymbol{\Psi}'_1 \right) . \hat{\mathbf{r}} \right] \tag{9}$$

where

$$\boldsymbol{\Psi}'_1 = \boldsymbol{\Psi}_1 - \Delta\mathbf{r}$$
$$\mathbf{H}'_1 = \mathbf{H}_1 - \Delta\mathbf{r} \tag{10}$$

Clearly, the degree-1 vector displacement function depends on the arbitrary choice of reference frame origin.

[9] Equation (10) implies that there exist special reference frames in which either the horizontal displacements or the vertical displacements are zero for degree-1 deformation [*Blewitt et al.*, 2001]. These are the CL (center of lateral figure) and CH (center of height figure) frames, respectively [*Blewitt*, 2003]. That the vertical degree-1 displacements can be made zero by a simple translation proves that the model Earth retains a shape of constant radius under a degree-1 deformation, and hence retains a perfect spherical shape. However, if $\mathbf{H}'_1 = 0$, in general $\boldsymbol{\Psi}'_1 = \boldsymbol{\Psi}_1 - \mathbf{H}_1 \neq 0$; so the surface is strained, as detected by GPS [*Blewitt et al.*, 2001] and by very long baseline interferometry [*Lavallée and Blewitt*, 2002].

[10] In GPS geodesy, station coordinate time series are in practice often published in an effective center of figure (CF) frame [*Dong et al.*, 1997], defined by no net translation of the Earth's surface, and realized through a rigid-body transformation at every epoch. In the CF frame, *Blewitt et al.* [2001, Figure 2] show maximum seasonal variations in the degree-1 height function of 3 mm. Integrating equation (8) over the sphere, the no net translation condition is satisfied when

$$\boldsymbol{\Psi}_1 = -\frac{1}{2} \mathbf{H}_1 \tag{11}$$

which can be derived by substituting the identity $\hat{\mathbf{r}} = (Y_{11}^{C}, Y_{11}^{S}, Y_{10}^{C})$ and using equation (A4). Hence degree 1 is a special case in that there are only 3 (not 6) free parameters. Combining equations (1), (7), and (11), the degree-1 east, north and height surface functions can be written

$$\begin{pmatrix} E_1(\Omega) \\ N_1(\Omega) \\ H_1(\Omega) \end{pmatrix} = \begin{pmatrix} -\frac{1}{2} & 0 & 0 \\ 0 & -\frac{1}{2} & 0 \\ 0 & 0 & 1 \end{pmatrix} \mathbf{G}(\Omega) \begin{pmatrix} H_{11}^{C} \\ H_{11}^{S} \\ H_{10}^{C} \end{pmatrix} \tag{12}$$

where we define

$$\mathbf{G}(\Omega) = \begin{pmatrix} -\sin\lambda & \cos\lambda & 0 \\ -\sin\varphi\cos\lambda & -\sin\varphi\sin\lambda & \cos\varphi \\ \cos\varphi\cos\lambda & \cos\varphi\sin\lambda & \sin\varphi \end{pmatrix} \tag{13}$$

which can be identified as the geocentric to topocentric coordinate rotation matrix. So we can write the degree-1

geocentric coordinate displacements in the CF frame as the matrix equation:

$$\mathbf{D}_1(\Omega) = \mathbf{G}^T(\Omega)\mathbf{diag}\left[-\tfrac{1}{2}, -\tfrac{1}{2}, +1\right] \cdot \mathbf{G}(\Omega)\mathbf{H} \tag{14}$$

[11] Equation (14) applies quite generally to nontoroidal deformations. For example, it would not apply to plate tectonics, but it would apply to loading models that satisfy the Love-Shida hypothesis. Our approach cleanly separates the kinematic spectral inversion problem from static/dynamic problems, which require assumptions on the spatial and temporal variation of Earth's mechanical properties.

2.4. Inversion Model

[12] The observation equations for a set of estimated station displacement coordinates $\mathbf{b}_i = (e_i\ n_i\ u_i)$ for stations $i = 1,\ldots, s$ at geographic locations Ω_i at a given epoch are given by the matrix equation:

$$\mathbf{b} = \mathbf{A}\mathbf{x} + \mathbf{v} \tag{15}$$

where $\mathbf{b}$ is a column matrix of the observed displacements for the entire network

$$\mathbf{b} = (\mathbf{b}_1\ \mathbf{b}_2 \cdots \mathbf{b}_s)^T \tag{16}$$

$\mathbf{x}$ is a column matrix of unknown parameters, which are the spectral coefficients of the height and poloidal surface functions

$$\mathbf{x} = \left(H_{11}^C H_{11}^S H_{10}^C \middle| H_{20}^C \cdots H_{\bar{n}\bar{n}}^S \middle| \Psi_{20}^C \cdots \Psi_{\bar{n}\bar{n}}^S\right)^T \tag{17}$$

Note that terms Ψ_{1m}^{Φ} are not included as free parameters due to the no net translation constraint, equation (11). $\mathbf{A}$ is the matrix of partial derivatives, which has the following block structure

and $\mathbf{v}$ is column matrix of station coordinate residuals.

[13] Let us assume the stochastic model

$$E(\mathbf{v}\mathbf{v}^T) = \mathbf{C} \tag{19}$$

where E is the expectation operator, and $\mathbf{C}$ is the covariance matrix associated with the estimated station coordinate displacements. The weighted least squares solution for the spectral coefficients is

$$\begin{aligned} \hat{\mathbf{x}} &= \mathbf{C}_\mathbf{x}\mathbf{A}^\mathrm{T}\mathbf{C}^{-1}\mathbf{b} \\ \mathbf{C}_\mathbf{x} &= \left(\mathbf{A}^\mathrm{T}\mathbf{C}^{-1}\mathbf{A}\right)^{-1} \end{aligned} \tag{20}$$

where $\mathbf{C}_\mathbf{x}$ is the formal covariance matrix of the estimated spectral coefficients. Given the estimated spectral coefficients $\hat{\Psi}_{nm}^{\Phi}, \hat{H}_{nm}^{\Phi}$, and matrix $\mathbf{C}_\mathbf{x}$, it is then straightforward to construct the estimated surface vector displacements, and propagate the errors to compute the formal uncertainty in modeled displacement at any location on the sphere.

2.5. Truncation Considerations

[14] For a truncation at degree $\bar{n}$, there are $\bar{n}(\bar{n}+2)$ spectral coefficients H_{nm}^{Φ}. It is therefore technically possible to estimate coefficients up to degree $\bar{n}$ with an absolute minimum of $s = \bar{n}(\bar{n}+2)$ stations (for a nondegenerate network configuration). So in principle a 100-station well-distributed network can be used to estimate spectral coefficients up to degree 9.

[15] In practice, truncation well below this technical limit can have its advantages as an effective spatial filter of errors in the station heights. Truncation even to a very low degree might be justified on the grounds that spherical harmonic functions are orthogonal over the entire Earth's surface, and so are effectively orthogonal for a well-distributed network. However, some level of bias will be present for actual network configurations, which could be assessed by covari-

$$\mathbf{A} = \left(\begin{array}{c|ccc|ccc} & 0 & \cdots & 0 & \dfrac{\partial_\lambda Y_{20}^C(\Omega_1)}{\cos\varphi_1} & \cdots & \dfrac{\partial_\lambda Y_{\bar{n}\bar{n}}^S(\Omega_1)}{\cos\varphi_1} \\ \begin{pmatrix} -\frac{1}{2} & 0 & 0 \\ 0 & -\frac{1}{2} & 0 \\ 0 & 0 & 1 \end{pmatrix} G(\Omega_1) & 0 & \cdots & 0 & \partial_\varphi Y_{20}^C(\Omega_1) & \cdots & \partial_\varphi Y_{\bar{n}\bar{n}}^S(\Omega_1) \\ & Y_{20}^C(\Omega_1) & \cdots & Y_{\bar{n}\bar{n}}^S(\Omega_1) & 0 & \cdots & 0 \\ \hline \vdots & & \vdots & & & \vdots & \\ \hline & 0 & \cdots & 0 & \dfrac{\partial_\lambda Y_{20}^C(\Omega_s)}{\cos\varphi_s} & \cdots & \dfrac{\partial_\lambda Y_{\bar{n}\bar{n}}^S(\Omega_s)}{\cos\varphi_s} \\ \begin{pmatrix} -\frac{1}{2} & 0 & 0 \\ 0 & -\frac{1}{2} & 0 \\ 0 & 0 & 1 \end{pmatrix} G(\Omega_s) & 0 & \cdots & 0 & \partial_\varphi Y_{20}^C(\Omega_s) & \cdots & \partial_\varphi Y_{\bar{n}\bar{n}}^S(\Omega_s) \\ & Y_{20}^C(\Omega_s) & \cdots & Y_{\bar{n}\bar{n}}^S(\Omega_s) & 0 & \cdots & 0 \end{array}\right) \tag{18}$$

Table 1. Load Love Numbers and Combinations to Degree 12[a]

Degree n	Surface Height h_n'	Geoid Height $1 + k_n'$	Surface Lateral l_n'	Surface Lateral: Surface Height $\left\|\frac{l_n'}{h_n'}\right\|$	Surface Height: Load Thickness $\frac{3\rho_S h_n'}{(2n+1)\rho_E}$	Geoid Height: Load Thickness $\frac{3\rho_S(1+k_n')}{(2n+1)\rho_E}$	Sea Level: Load Thickness $\frac{3\rho_S(1+k_n'-h_n')}{(2n+1)\rho_E}$
1[b]	−0.269	1.021	0.134	0.500	−0.050	0.190	0.240
2	−1.001	0.693	0.030	0.029	−0.112	0.077	0.189
3	−1.052	0.805	0.074	0.071	−0.084	0.064	0.148
4	−1.053	0.868	0.062	0.059	−0.065	0.054	0.119
5	−1.088	0.897	0.049	0.045	−0.055	0.045	0.101
6	−1.147	0.911	0.041	0.036	−0.049	0.039	0.088
7	−1.224	0.918	0.037	0.030	−0.046	0.034	0.080
8	−1.291	0.925	0.034	0.026	−0.042	0.030	0.073
9	−1.366	0.928	0.032	0.023	−0.040	0.027	0.067
10	−1.433	0.932	0.030	0.021	−0.038	0.025	0.063
11	−1.508	0.934	0.030	0.020	−0.037	0.023	0.059
12	−1.576	0.936	0.029	0.018	−0.035	0.021	0.056

[a]Columns 2–4 are computed from *Farrell* [1972] (interpolated for degrees 7, 9, 11, and 12). Load thickness is defined as the height of a column of seawater, specific density 1.025.

[b]Frame-dependent degree-1 numbers computed in center of figure (CF) frame [*Blewitt et al.*, 2001], except for sea level:load thickness, which is frame-invariant. Degree-1 numbers should be transformed into the isomorphic frame adopted by a specific investigation [*Blewitt*, 2003].

ance analysis. In the case of low-degree truncation, high-degree signal components would tend to be absorbed into the station displacement residuals. Conversely, in the case of high-degree truncation, the higher-degree estimates would tend to absorb some of the station position errors. It may be effective to estimate as many degrees as technically possible, but only interpret the results up to a degree less than $\overline{n}$; such considerations would need to be investigated.

[16] In principle it should be possible to assess the precision of the spectral coefficients by comparing independent estimates of the load inversion (described below) that use only H_{nm}^{Φ} or Ψ_{nm}^{Φ}, and use this to guide the selection of truncation degree $\overline{n}$, or to improve the stochastic model. The selection of $\hat{n}$ is not discussed further here, except to note that a standard F test might be used to assess whether adding an extra degree to the model produces a statistically significant decrease in the residual variance.

3. Spectral Inversion for Mass Distribution

3.1. Surface Mass Redistribution

[17] Consider a spherical solid Earth of radius a, plus surface mass that is free to redistribute in a thin surface layer ($\ll a$). Without loss of generality, we can simplify the equations by expressing the total surface density of this layer (irrespective of its composition) as the equivalent height of a column of seawater $T(\Omega)$. That is, the surface mass per unit area everywhere is by definition $\rho_S T(\Omega)$ where the density of seawater is taken to be $\rho_S = 1025$ kg m^{-3}.

[18] On land, $T(\Omega)$ would include both the local variation in atmospheric pressure and continental water. Over the oceans, in the absence of steric effects and atmospheric interactions, $T(\Omega)$ can be considered the value of static sea level. It depends on the application as to whether the effect of atmospheric pressure on sea level is an important consideration. For example, under the inverse barometer assumption, a change in atmospheric mass distribution tends to produce an opposite change in oceanic mass distribution, thus over the oceans, geographic variations in $T(\Omega)$ are not strongly sensitive to the atmospheric component (although $T(\Omega)$ would include the variation in atmospheric pressure averaged over the oceans). On the other hand, if the application requires that estimates of $T(\Omega)$ be geometrically interpreted as sea level, then such sea level predictions would be strongly sensitive to atmospheric pressure (except for global mean sea level, which is unaffected). *Van Dam et al.* [1997] show how to calculate the effect of atmospheric pressure on sea level. In this paper, we simplify this aspect of the discussion by assuming that the application does not require us to consider the atmospheric component of $T(\Omega)$, and so we loosely refer to $T(\Omega)$ over the ocean as sea level, and over the land as continental water. This does not invalidate the equations, assuming that the variations in the total mass of the atmosphere (due to water vapor) are negligible [*Trenberth*, 1981].

3.2. Static Spectral Displacement Model

[19] Let us consider the total mass distribution function as a spherical harmonic expansion:

$$T(\Omega) = \sum_{n=1}^{\infty}\sum_{m=0}^{n}\sum_{\Phi}^{\{C,S\}} T_{nm}^{\Phi} Y_{nm}^{\Phi}(\Omega) \tag{21}$$

The summation begins at degree $n = 1$ because we assume that, although the surface load can be redistributed, its total mass is conserved.

[20] Such a surface load changes the gravitational potential on the surface of a rigid, spherical Earth by an amount [*Farrell*, 1972]:

$$\begin{aligned} V_T(\Omega) &= \sum_{n=1}^{\infty}\sum_{m=0}^{n}\sum_{\Phi}^{\{C,S\}} \frac{4\pi G a}{(2n+1)}\rho_S T_{nm}^{\Phi} Y_{nm}^{\Phi}(\Omega) \\ &= \sum_{n=1}^{\infty}\sum_{m=0}^{n}\sum_{\Phi}^{\{C,S\}} \frac{3g\rho_S}{(2n+1)\rho_E} T_{nm}^{\Phi} Y_{nm}^{\Phi}(\Omega) \end{aligned} \tag{22}$$

where G is the gravitational constant, the Earth's radius a = 6371 km (which equates the volume and surface area of our model sphere to that of the conventional reference ellipsoid), and g is acceleration due to gravity. Assuming the Earth's mass is 5.973×10^{24} kg, the mean density of the Earth is $\rho_E = 5514$ kg m^{-3}. For a spherically symmetric elastic Earth model, the load deforms the Earth and changes

its self-gravitation, thus creating an additional potential on the (original) reference surface

$$V_K(\Omega) = \sum_{n=1}^{\infty} k'_n [V_T(\Omega)]_n = \sum_{n=1}^{\infty}\sum_{m=0}^{n}\sum_{\Phi}^{\{C,S\}} k'_n \frac{3g\rho_S}{(2n+1)\rho_E} T^{\Phi}_{nm} Y^{\Phi}_{nm}(\Omega) \quad (23)$$

where k'_n is the gravitational static degree n load Love number [*Farrell*, 1972].

[21] Let us carefully define "the geoid" as the equipotential surface with the same potential as that of the sea surface on the undeformed model Earth. That is, by our definition, the geoid is allowed to deform due to redistribution of mass, but it must retain its same potential. For future reference in our model of sea level, the height of the geoid above the reference surface (the initial geoid) is given everywhere by

$$N(\Omega) = \frac{1}{g}[V_T(\Omega) + V_K(\Omega)] = \sum_{n=1}^{\infty}\sum_{m=0}^{n}\sum_{\Phi}^{\{C,S\}} (1+k'_n)\frac{3\rho_S}{(2n+1)\rho_E} T^{\Phi}_{nm} Y^{\Phi}_{nm}(\Omega) \quad (24)$$

Table 1 shows the geoid height load Love number $(1 + k'_n)$ along with other Love numbers and useful combinations to degree 12, derived from *Farrell* [1972]. For example, the coefficient in equation (24) is shown in Table 1 as ratio "geoid height: load thickness."

[22] In this paper, we have used Love numbers from *Farrell* [1972], which refer to a symmetric, no-rotating elastic, isotropic (SNREI) Earth model based on the Gutenberg-Bullen A model. Farrell's Love numbers are widely used in the geodetic community, for example, in elastic Green's function models of hydrological and atmospheric loading [*van Dam et al.*, 2001]. The preliminary reference Earth model PREM [*Dziewonski and Anderson*, 1981] yields low-degree load Love numbers almost identical to Farrell's [*Lambeck*, 1988; *Grafarend et al.*, 1997]. More general classes of Earth model have been discussed by *Plag et al.* [1996]. *Mitrovica et al.* [1994] and *Blewitt* [2003] have further discussions on model and reference frame considerations. For the inversion of seasonal loading, mechanical model considerations are relatively minor compared to limitations of the load model and its spatial resolution.

[23] Using the load Love number formalism the height spectral coefficients can be derived by

$$H(\Omega) = \sum_{n=1}^{\infty}\frac{h'_n}{g}[V_T(\Omega)]_n = \sum_{n=1}^{\infty}\sum_{m=0}^{n}\sum_{\Phi}^{\{C,S\}} h'_n \frac{3\rho_S}{(2n+1)\rho_E} T^{\Phi}_{nm} Y^{\Phi}_{nm}(\Omega)$$
$$H^{\Phi}_{nm} = h'_n \frac{3\rho_S}{(2n+1)\rho_E} T^{\Phi}_{nm} \quad (25)$$

where h'_n are the height load Love numbers. The term $(2n+1)$ in the denominator of equation (25), coupled with the knowledge that h'_n asymptotically approaches a constant as $n \rightarrow \infty$ (the elastic half-space Boussinesq problem [*Farrell*, 1972]), indicates that mass distribution coefficients T^{Φ}_{nm} become increasingly sensitive to errors in the height coefficients for increasing degree n. This underscores our suggesting a conservatively low choice of truncation degree $\overline{n}$.

[24] The poloidal spectral coefficients are derived by first expressing the poloidal component of lateral displacement in equation (2) as a function of the loading potential according to load Love number theory:

$$\nabla\Psi(\Omega) = \sum_{n=1}^{\infty}\frac{l'_n}{g}\nabla[V_T(\Omega)]_n$$
$$\Psi(\Omega) = \sum_{n=1}^{\infty}\frac{l'_n}{g}[V_T(\Omega)]_n + \Psi^C_{00} = \sum_{n=1}^{\infty}\sum_{m=0}^{n}\sum_{\Phi}^{\{C,S\}} l'_n \frac{3\rho_S}{(2n+1)\rho_E} T^{\Phi}_{nm} Y^{\Phi}_{nm}(\Omega) \quad (26)$$
$$\Psi^{\Phi}_{nm} = l'_n \frac{3\rho_S}{(2n+1)\rho_E} T^{\Phi}_{nm}$$

where l'_n are the lateral load Love numbers, and where (as before) we set the integration constant $\Psi^c_0 = 0$ without affecting the actual displacements in equation (2).

[25] Table 1 gives the ratio "surface height: load thickness" up to degree 12. It also gives the ratio "surface lateral: surface height," which is the ratio of lateral to height load Love numbers. For the special case of degree 1 in the CF frame, equation (11) implies $l'_1/h'_1 = -1/2$ for all spherically symmetric models that obey the Love-Shida hypothesis. With the exception of degree 1, the relative contribution of horizontal data suffers from the low surface lateral to surface height displacement ratio, which for degrees 2 to 9 ranges from 0.02 to 0.07 (peaking at degree 3). However, the simultaneous inversion of poloidal data can be justified because the ratio of horizontal to vertical variance is typically small for globally referenced coordinates ($\sim$0.1) [*Davies and Blewitt*, 2000]; thus the relative information content of horizontal displacements can be significant, despite the low-magnitude Love numbers [*Mitrovica et al.*, 1994].

3.3. Inversion Model

[26] From the above development, the spectral coefficients for the observed surface displacement functions can be modeled

$$\hat{\mathbf{x}} = \mathbf{B}\mathbf{y} + \mathbf{v}_{\mathbf{x}} \quad (27)$$

where $\hat{\mathbf{x}}$, given by equation (20), contains estimated spectral coefficients of displacement according to the structure of equation (17); $\mathbf{y}$ is a column matrix of unknown parameters, which are the spectral coefficients of the mass distribution function

$$\mathbf{y} = \left(T^C_{11}\ T^S_{11}\ T^C_{10} \mid T^C_{20} \cdots\ T^S_{\bar{n}\bar{n}}\right)^T \quad (28)$$

$\mathbf{B}$ is the matrix of partial derivatives which has a diagonal block structure

$$\mathbf{B} = \frac{3\rho_S}{(2n+1)\rho_E}\left(\begin{array}{c|ccc} h'_1\mathbf{I}_3 & 0 & \cdots & 0 \\ \hline 0 & h'_2\mathbf{I}_5 & & \\ \vdots & & \ddots & \\ 0 & & & h'_{\bar{n}}\mathbf{I}_{2\bar{n}+1} \\ \hline 0 & l'_2\mathbf{I}_5 & & \\ \vdots & & \ddots & \\ 0 & & & l'_{\bar{n}}\mathbf{I}_{2\bar{n}+1} \end{array}\right) \quad (29)$$

Table 2. Ocean Function Spectral Coefficients Used in This Analysis[a]

Coefficient C^{Φ}_{nm}	Degree 0 C^{Φ}_{0m}	Degree 1 C^{Φ}_{1m}	Degree 2 C^{Φ}_{2m}	Degree 3 C^{Φ}_{3m}	Degree 4 C^{Φ}_{4m}
C^{C}_{n0}	0.69700	−0.21824	−0.13416	0.11906	−0.07200
C^{C}_{n1}		−0.18706	−0.05164	0.04753	0.03415
C^{S}_{n1}		−0.09699	−0.06584	−0.03456	0.02846
C^{C}_{n2}			0.02582	0.02391	0.02012
C^{S}_{n2}			0.00129	−0.03040	−0.00470
C^{C}_{n3}				−0.00223	−0.00317
C^{S}_{n3}				−0.01241	0.00030
C^{C}_{n4}					0.00030
C^{S}_{n4}					−0.00213

[a]Normalization removed from coefficients of *Balmino et al.* [1973]. Convention for unnormalized coefficients in Appendix A.

and $\mathbf{v_x}$ is column matrix of displacement coefficient residuals.

[27] Let us assume the stochastic model

$$E\left(\mathbf{v_x}\mathbf{v_x}^T\right) = \mathbf{C_x} \tag{30}$$

where $\mathbf{C_x}$ is given by equation (20). The weighted least squares solution for the mass distribution spectral coefficients is

$$\begin{aligned} \hat{\mathbf{y}} &= \mathbf{C_y}\mathbf{B}^{\mathrm{T}}\mathbf{C_x}^{-1}\hat{\mathbf{x}} \\ \mathbf{C_y} &= \left(\mathbf{B}^{\mathrm{T}}\mathbf{C_x}^{-1}\mathbf{B}\right)^{-1} \end{aligned} \tag{31}$$

where $\mathbf{C_Y}$ is the formal covariance matrix of the estimated mass distribution coefficients.

[28] The two-step estimation process prescribed by equations (20) and (31) would in principle give an identical solution as a one-step process. It is convenient to break the solution into two steps because, as previously discussed, the first step is independent of load Love numbers derived from specific models. More specifically, it is useful to assess from the first step how well the truncated spectral model fits the original station displacement data, and to reject outliers or improve the stochastic model using formal statistical procedures that do not rely on the validity of specific loading models. The second step might be applied separately multiple times using different sets of load Love numbers from various models, or to assess, for example, how consistent are the poloidal and height spectral coefficients. In principle the mass distribution spectral coefficients can be estimated using only height spectral coefficients or only poloidal coefficients, thus providing an alternative assessment of the stochastic model.

3.4. Ocean-Landmass Exchange and Global Mean Sea Level

[29] One useful result that can be derived immediately is the total mass exchanged between the oceans and the continents. The effect of ocean-landmass exchange on change in global mean sea level is

$$\bar{S} = \frac{\iint_{\text{ocean}} T(\Omega)d\Omega}{\iint_{\text{ocean}} d\Omega} = \sum_{n=1}^{\infty}\sum_{m=0}^{n}\sum_{\Phi}^{\{C,S\}} \frac{C^{\Phi}_{nm}T^{\Phi}_{nm}}{C^{C}_{00}\Pi^{2}_{nm}} \tag{32}$$

where C^{Φ}_{nm} are spectral coefficients of the ocean function $C(\Omega)$, which takes the value 1 over the oceans and 0 on land [*Munk and MacDonald*, 1960], and the normalization coefficient Π_{nm} is defined in Appendix A. The ocean function coefficients can be computed to some finite degree using coastline data [*Balmino et al.*, 1973] according to

$$C^{\Phi}_{nm} = \frac{\Pi^{2}_{nm}}{4\pi}\iint_{\text{ocean}} Y^{\Phi}_{nm}d\Omega \tag{33}$$

[30] Table 2 shows unnormalized ocean function coefficients up to degree 4, consistent with our convention in Appendix A. *Chao and O'Connor* [1988] urge us to be careful due to pervasive "errors which arose from normalization conventions" in the literature. The coefficients from *Balmino et al.* [1973] (later reproduced by *Lambeck* [1980]) were chosen because two independent analysis groups using different conventions corroborated the values. Published coefficients by *Munk and MacDonald* [1960] have been questioned by *Balmino et al.* [1973], and appear to us to contain errors associated with inconsistent application of normalization conventions. The coefficients by *Dickman* [1989], while they may derive from more accurate satellite data, appear to be fundamentally inconsistent with the ocean function's idempotent nature, and higher order coefficients appear to be systematically too small (by orders of magnitude), which again suggests normalization problems.

[31] Using equations (32) and (33) the mass taken from the ocean and deposited on land is

$$\Delta M = -\rho_S\bar{S}a^2\iint_{\text{ocean}} d\Omega = -4\pi a^2\rho_S\sum_{n=1}^{\infty}\sum_{m=0}^{n}\sum_{\Phi}^{\{C,S\}}\frac{C^{\Phi}_{nm}T^{\Phi}_{nm}}{\Pi^{2}_{nm}} \tag{34}$$

Global mean sea level is only sensitive to low-degree mass redistribution (because it involves the square of spectral coefficients that obey a naturally decreasing power law) and so truncation of equations (32) and (34) is a relatively minor issue.

4. Spatial Inversion for Mass Distribution

4.1. Model-Free Inversion

[32] Without any a priori knowledge of the dynamics of mass redistribution, a naïve model-free solution to the spatial distribution of mass is given by equation (21)

$$\hat{T}(\Omega) = \sum_{n=1}^{\bar{n}}\sum_{m=0}^{n}\sum_{\Phi}^{\{C,S\}}\hat{T}^{\Phi}_{nm}Y^{\Phi}_{nm}(\Omega) \tag{35}$$

where estimates for the mass distribution coefficients are given by equation (31). Ideally, if we knew all the values of the infinite number of total mass distribution coefficients T^{Φ}_{nm} then sea level $S(\Omega)$ would be given straightforwardly by using the ocean function:

$$S(\Omega) = C(\Omega)T(\Omega) = C(\Omega)\sum_{n=1}^{\infty}\sum_{m=0}^{n}\sum_{\Phi}^{\{C,S\}}T^{\Phi}_{nm}Y^{\Phi}_{nm}(\Omega) \tag{36}$$

Similarly, the continental mass distribution $L(\Omega)$ would be given by

$$L(\Omega) = [1 - C(\Omega)]T(\Omega) = [1 - C(\Omega)] \sum_{n=1}^{\infty} \sum_{m=0}^{n} \sum_{\Phi}^{\{C,S\}} T_{nm}^{\Phi} Y_{nm}^{\Phi}(\Omega) \tag{37}$$

so that

$$T(\Omega) = S(\Omega) + L(\Omega) \tag{38}$$

(where $L(\Omega)$ refers to the equivalent height of a column of seawater on land).

[33] A problem with the above approach is that the coefficients $\hat{T}_{nm}^{\Phi}$ are in practice only given to a finite degree $\overline{n}$ so the real discontinuity of mass distribution at the coastlines is poorly represented by a smooth function. A more serious objection is that a model of sea level formed by truncating equation (36) will not even approximately conform to an equipotential surface, and so is physically unreasonable. Next we shall address this by incorporating the physics of how the oceans respond passively to changes in the Earth's surface potential from mass redistribution.

4.2. Relative Sea Level in Static Equilibrium

[34] In hydrostatic equilibrium, the upper surface of the ocean adopts an equipotential surface. Equilibrium tidal theory neglects ocean currents associated with any change in sea level, and so is presumed to be valid for periods longer than the time constant associated with tidal friction, [*Proudman*, 1960; *Munk and MacDonald*, 1960] and therefore should be applicable to fortnightly periods and beyond [*Agnew and Farrell*, 1978]. For our intended application of the theory we shall now develop, we are mainly concerned with the forcing of sea level by the seasonal to decadal-scale loading due to continental water storage, and so we assume the static equilibrium model.

[35] Let us define "relative sea level" as the column height of the ocean as measured from the solid Earth surface at the ocean's bottom to the ocean's upper surface. The change in relative sea level from an initial equilibrium state to a new equilibrium state can be expressed, to within a constant, as the change in height of the geoid relative to the underlying model of the Earth's surface. In its most general form [*Dahlen*, 1976], relative sea level $S(\Omega)$ in static equilibrium is the following function of geographical position Ω

$$S(\Omega) = C(\Omega)(N(\Omega) - H(\Omega) + \Delta V/g) \tag{39}$$

where the geoid height $N(\Omega)$ is given by equation (24); and $C(\Omega)H(\Omega)$ is the height of the deformed ocean basins, given by equation (25). The constant $\Delta V/g$ is required because, although the sea surface will relax to an equipotential surface, it will generally have a different potential to its initial potential, depending on the total oceanic mass and the irregular ocean-land distribution [*Dahlen*, 1976]. Therefore ΔV represents the geopotential of the sea surface relative to the geoid's potential, and $\Delta V/g$ represents the height of the sea surface above the deformed geoid.

[36] Inserting equations (24) and (25) into (39) gives us "the sea level equation" appropriate to our problem:

$$S(\Omega) = C(\Omega)\left[\sum_{n=1}^{\infty} \sum_{m=0}^{n} \sum_{\Phi}^{\{C,S\}} \frac{3\left(1 + k_n' - h_n'\right)\rho_S}{(2n+1)\rho_E} T_{nm}^{\Phi} Y_{nm}^{\Phi}(\Omega) + \frac{\Delta V}{g}\right] \tag{40}$$

The total load coefficients T_{nm}^{Φ} themselves include a contribution from sea level and so traditionally equations similar to (40) have been either inverted [*Dahlen*, 1976] or solved iteratively [*Wahr*, 1982; *Mitrovica et al.*, 1994], given an applied nonoceanic load (or tidal potential).

[37] Indeed such a calculation would be appropriate if we were to compute how the ocean's passive response modifies the effect of a given land load on the Earth's shape (something that is generally not accounted for in current loading models). However, in our application we have direct access to estimates $\hat{T}_{nm}^{\Phi}$ and so have no need to solve the sea level equation in the same sense. Our estimate for sea level at a given location can therefore be written

$$\hat{S}(\Omega) = C(\Omega)\widetilde{S}(\Omega) \tag{41}$$

where we define the quasi-spectral sea level function

$$\tilde{S}(\Omega) = \sum_{n=1}^{\bar{n}} \sum_{m=0}^{n} \sum_{\Phi}^{\{C,S\}} \frac{3\left(1 + k_n' - h_n'\right)\rho_S}{(2n+1)\rho_E} \hat{T}_{nm}^{\Phi} Y_{nm}^{\Phi}(\Omega) + \frac{\Delta V}{g} \tag{42}$$

[38] "Quasi-spectral" implies that the coefficients of this function apply over the oceanic spatial domain rather than the global spatial domain, and it indicates the coefficients are intended for spatial interpretation through equation (41); expressions for the global spectral coefficients are derived later. The coefficient in equation (42) is given in Table 1 as "sea level: load thickness" to degree 12.

[39] We now evaluate the sea surface geopotential ΔV subject to the mass exchange condition given by equation (34). Integrating equation (41) over the sphere, we find the degree-0 global spectral coefficient is

$$\hat{S}_{00}^{C} = \sum_{n=1}^{\bar{n}} \sum_{m=0}^{n} \sum_{\Phi}^{\{C,S\}} \frac{3\left(1 + k_n' - h_n'\right)\rho_S}{(2n+1)\rho_E} \frac{C_{nm}^{\Phi} \hat{T}_{nm}^{\Phi}}{\Pi_{nm}^2} + \frac{\Delta V}{g} C_{00}^{C} \tag{43}$$

Now from our previous discussion on mass exchange, we must satisfy the condition

$$\hat{S}_{00}^{C} = \iint_{\text{ocean}} \hat{T}(\Omega) d\Omega = \sum_{n=1}^{\bar{n}} \sum_{m=0}^{n} \sum_{\Phi}^{\{C,S\}} \frac{C_{nm}^{\Phi} \hat{T}_{nm}^{\Phi}}{\Pi_{nm}^2} = -\hat{L}_{00}^{C} \tag{44}$$

and so equating (43) and (44),

$$\frac{\Delta V}{g} = \sum_{n=1}^{\bar{n}} \sum_{m=0}^{n} \sum_{\Phi}^{\{C,S\}} \left[1 - \frac{3\left(1 + k_n' - h_n'\right)\rho_S}{(2n+1)\rho_E}\right] \frac{C_{nm}^{\Phi} \hat{T}_{nm}^{\Phi}}{C_{00}^{C} \Pi_{nm}^2} = \widetilde{S}_{00}^{C} \tag{45}$$

where the first term in the square bracket is related to change in global mean sea level from mass exchange, and the smaller second term (previously derived by *Dahlen*

[1976]) is the contribution of average geoid and seafloor deformation, which is generally nonzero even in the absence of mass exchange. When using equation (41) for interpreting sea level at any point, it is important to use the spatial rather than spectral representation of the ocean function, because $\hat{S}(\Omega)$ must go discontinuously to zero as we cross a coastline toward land.

4.3. Geocentric Sea Level and Static Topography

[40] We now digress to discuss sea level as inferred by satellite altimetry. Satellite altimetry of the ocean surface is inherently sensitive to geocentric sea level rather than relative sea level. Perhaps misleadingly, geocentric sea level has been referred to as "absolute sea level," when in fact, it is dependent on the choice of reference frame origin; ironically, relative sea level is absolute in this sense, as it is frame-independent. To be truly self-consistent, the coordinates of the tracking stations used to determine the geocentric satellite position should be allowed to move with the loading deformation, for example using the same epoch coordinates as those used to estimate the total load. The ocean's dynamic topography used to investigate ocean currents can be derived if we know the height of the sea surface above the ocean's static topography. For purposes of our problem, the ocean's static topography may be defined as the geocentric height of the ocean surface in hydrostatic equilibrium if there were no ocean currents or steric effects. Contributing factors therefore include the deformation of the geoid and the difference in potential between the deformed geoid and the new sea surface. We formally define the ocean's static topography using this new equipotential surface which is given everywhere as

$$\tilde{O}(\Omega) = N(\Omega) + \Delta V/g \tag{46}$$

where $\Delta V/g$ can be estimated by equation (45) and the geoid height can be estimated by

$$\hat{N}(\Omega) = \sum_{n=1}^{\bar{n}} \sum_{m=0}^{n} \sum_{\Phi}^{\{C,S\}} \left(1 + k'_n\right) \frac{3\rho_S}{(2n+1)\rho_E} \hat{T}^{\Phi}_{nm} Y^{\Phi}_{nm}(\Omega) \tag{47}$$

Using equation (46) it is straightforward to calculate the mean change in sea level in a geocentric frame (where the degree-1 load Love numbers must be consistent with the type of geocentric frame used to derive the altimeter coordinates [*Blewitt*, 2003]),

$$\bar{O} = \frac{\iint_{\text{ocean}} \tilde{O}(\Omega) d\Omega}{\iint_{\text{ocean}} d\Omega} = \sum_{n=1}^{\infty} \sum_{m=0}^{n} \sum_{\Phi}^{\{C,S\}} \frac{C^{\Phi}_{nm} \tilde{O}^{\Phi}_{nm}}{C^C_{00} \Pi^2_{nm}}$$
$$= \sum_{n=1}^{\infty} \sum_{m=0}^{n} \sum_{\Phi}^{\{C,S\}} \left[1 + \frac{3h'_n \rho_S}{(2n+1)\rho_E}\right] \frac{C^{\Phi}_{nm} \hat{T}^{\Phi}_{nm}}{C^C_{00} \Pi^2_{nm}} = \bar{S} + \bar{H} \tag{48}$$

where explicitly shown is the intuitive notion that mean geocentric sea level $\overline{O}$ is the sum of mean relative sea level $\bar{S}$, given by equation (32), and the mean height change of the ocean floor $\overline{H}$, where H is given by equation (25). It can be seen from Table 1 (surface height: load thickness ratio) that geocentric and relative mean sea level only differ by a few percent (at most 11.2% for pure degree 2), which is not surprising since the seafloor is deformed an order of magnitude less than the change in sea level. Therefore the cautionary remark above regarding the treatment of station locations for satellite altimetry is only important at this level.

4.4. Linearized Sea Level Equation

[41] Before we solve for the land load, it will be necessary to find the global spectral coefficients of equation (41). This is the most computationally difficult part of the calculation. We make use of the fact that, as for any function on a sphere, the product of two spherical harmonics must itself be expressible as a spherical harmonic expansion. The product-to-sum conversion formula for spherical harmonics is [*Balmino*, 1994]

$$Y^{\Phi'}_{n'm'}(\Omega) Y^{\Phi''}_{n''m''}(\Omega) = \sum_{n=0}^{\infty} \sum_{m=0}^{n} \sum_{\Phi}^{\{C,S\}} A^{\Phi,\Phi',\Phi'}_{nm,n'm',n''m'} Y^{\Phi}_{nm}(\Omega) \tag{49}$$

where the coefficients can be expressed by applying equation (A6):

$$A^{\Phi,\Phi',\Phi''}_{nm,n'm',n''m''} = \frac{\Pi^2_{nm}}{4\pi} \oint\!\!\oint Y^{\Phi}_{nm}(\Omega) Y^{\Phi''}_{n'm'}(\Omega) Y^{\Phi''}_{n'm''}(\Omega) d\Omega \tag{50}$$

The integral of triple complex spherical harmonics arises in angular momentum theory of quantum mechanics [*Wigner*, 1959], and can be solved using Clebsch-Gordan coefficients or Wigner 3-*j* coefficients [*Dahlen*, 1976; *Balmino*, 1994]. Appendix B shows our method for the case of classical spherical harmonics. Once calculated, these integrals can be used to determine the global spectral coefficients for relative sea level, given the quasi-spectral coefficients. The ocean function product-to-sum conversion can be derived using equation (49):

$$C(\Omega)\widetilde{S}(\Omega) = \sum_{n'm'\Phi'} \sum_{n''m''\Phi''} C^{\Phi''}_{n''m''} \widetilde{S}^{\Phi'}_{n'm'} Y^{\Phi'}_{n'm'}(\Omega) Y^{\Phi''}_{n''m''}(\Omega)$$
$$= \sum_{nm\Phi} \sum_{n'm'\Phi'} \sum_{n''m''\Phi''} C^{\Phi''}_{n''m''} \widetilde{S}^{\Phi'}_{n'm'} A^{\Phi,\Phi',\Phi''}_{nm,n'm',n''m''} Y^{\Phi}_{nm}(\Omega) \tag{51}$$

or alternatively in coefficient form as a matrix equation [e.g., *Dickman*, 1989, equation (14)]:

$$[C(\Omega)\tilde{S}(\Omega)]^{\Phi}_{nm} = \sum_{n'm'\Phi'} \mathrm{X}^{\Phi,\Phi'}_{nm,n'm'} \widetilde{S}^{\Phi'}_{n'm'} \tag{52}$$

where we define the coefficients of the product-to-sum transformation:

$$\mathrm{X}^{\Phi,\Phi'}_{nm,n'm'} = \sum_{n''=0}^{\infty} \sum_{m''=0}^{n''} \sum_{\Phi''}^{\{C,S\}} A^{\Phi,\Phi',\Phi''}_{nm,n'm',n''m''} C^{\Phi''}_{n''m''} \tag{53}$$

That is, multiplication of a function by the ocean function can be achieved by a linear transformation of that function's coefficients. Appendix B shows explicitly how equation (52) is actually computed by a recursive algorithm, and

Table 3. Product-to-Sum Transformation Coefficients[a]

$X^{\Phi,\Phi'}_{nm,n'm'}$	n′,m′,Φ′								
n,m,Φ	0,0,*C*	1,0,*C*	1,1,*C*	1,1,*S*	2,0,*C*	2,1,*C*	2,1,*S*	2,2,*C*	2,2,*S*
0,0,*C*	0.697	−0.073	−0.062	−0.032	−0.027	−0.031	−0.040	0.062	0.003
1,0,*C*	−0.218	0.643	−0.031	−0.040	−0.057	−0.063	−0.094	0.123	−0.156
1,1,*C*	−0.187	−0.031	0.755	0.002	0.062	−0.100	−0.078	−0.283	−0.290
1,1,*S*	−0.097	−0.040	0.002	0.693	0.002	−0.078	−0.223	−0.093	−0.214
2,0,*C*	−0.134	−0.094	0.103	0.003	0.638	0.027	0.012	0.084	−0.045
2,1,*C*	−0.052	−0.035	−0.056	−0.043	0.009	0.771	−0.012	−0.124	−0.064
2,1,*S*	−0.066	−0.052	−0.043	−0.124	0.004	−0.012	0.612	0.076	0.003
2,2,*C*	0.026	0.017	−0.039	−0.013	0.007	−0.031	0.019	0.744	−0.085
2,2,*S*	0.001	−0.022	−0.040	−0.030	−0.004	−0.016	0.001	−0.085	0.720

[a]Transformation defined by equation (53), with computational method shown in Appendices B and C. Calculation uses ocean function coefficients from Table 2. The strong diagonal nature is evident.

Appendix C presents results of this calculation up to degree 2 (as a check for readers wishing to reproduce our results or apply our method). Table 3 shows the product-to-sum transformation coefficients for spectral interactions to degree 2 × degree 2 assuming the ocean function coefficients of *Balmino et al.* [1973].

[42] Because of selection rules on indices that lead to nonzero integrals, the inner summation over double-primed indices involves only a limited number of contributing terms. As *Dahlen* [1976] points out, one result of this is that the ocean function is only required to degree $2n$ for an exact computation of its effect on an arbitrary degree-n function. Thus the spherical harmonic formulation is especially well suited for the investigation of low-degree phenomena.

[43] It should be emphasized that truncation implies that a sea level function constructed spatially using global spectral coefficients will generally be nonzero on land. This is why the quasi-spectral sea level function is recommended for spatial representation of sea level. However, we need the true spectral coefficients to compute the contribution of sea level to the observed total deformation.

4.5. Inversion for Continental Mass Redistribution

[44] The principle behind the following procedure is that spectral coefficients are applicable to the physics of loading, but quasi-spectral coefficients characterize the spatial distribution. Using sea level's spectral coefficients, we can subtract the sea level's contribution from the observed total deformation, and thus infer the continental load's spectral coefficients. Then the continental load's spectral coefficients can be inverted for quasi-spectral coefficients, which can be used to infer the continental load in the spatial domain.

[45] Formally, spectral coefficients for the land load up to degree $\bar{n}$ can be estimated as

$$\hat{L}^{\Phi}_{nm} = \hat{T}^{\Phi}_{nm} - \hat{S}^{\Phi}_{nm} \tag{54}$$

where $\hat{S}^{\Phi}_{nm}$ is given by equation (41). For spatial representation, the quasi-spectral land load function $\widetilde{L}(\Omega)$ satisfies the following equation:

$$\hat{L}(\Omega) = [1 - C(\Omega)]\widetilde{L}(\Omega) \tag{55}$$

such that the spectral coefficients are the same on both sides of this equation up to degree $\bar{n}$. Equating the spectral coefficients, we find that

$$\hat{L}^{\Phi}_{nm} = \sum_{n'=0}^{\bar{n}} \sum_{m'=0}^{n'} \sum_{\Phi'}^{\{C,S\}} \left(\delta^{\Phi,\Phi'}_{nm;n'm'} - X^{\Phi,\Phi'}_{nm;n'm'} \right) \widetilde{L}^{\Phi'}_{n'm'} \tag{56}$$

Thus equating (54) with (56) relates the quasi-spectral coefficients $\widetilde{L}^{\Phi}_{nm}$ to the estimated load coefficients $\hat{T}^{\Phi}_{nm}$. To find $\widetilde{L}^{\Phi}_{nm}$ up to degree $\bar{n}$ requires inversion of the matrix form of equation (56). Once we find $\widetilde{L}^{\Phi}_{nm}$, we can then construct the land load spatially using equation (55).

4.6. Reconstruction of the Total Load at Higher Degrees

[46] Equation (54) guarantees that our model for land and ocean mass redistribution yields spectral coefficients for the total load that agree with our original estimates $\hat{T}^{\Phi}_{nm}$ for $n = 1,\ldots\bar{n}$. However, note that equations (54) and (56) can be used to predict higher-degree coefficients $n > \bar{n}$ of the total load, because there is no restriction in these equations on the value of n.

$$\hat{T}(\Omega) = C(\Omega)\widetilde{S}(\Omega) + [1 - C(\Omega)]\widetilde{L}(\Omega)$$

$$\hat{T}^{\Phi}_{nm} = \sum_{n'=0}^{\bar{n}} \sum_{m'=0}^{n'} \sum_{\Phi'}^{\{C,S\}} \left[X^{\Phi,\Phi'}_{nm;n'm'} \widetilde{S}^{\Phi'}_{n'm'} + \left(\delta^{\Phi,\Phi'}_{nm;n'm'} - X^{\Phi,\Phi'}_{nm;n'm'} \right) \widetilde{L}^{\Phi'}_{n'm'} \right] \tag{57}$$

Whether these predicted values are physically meaningful depends on the underlying model assumptions that provide the "extra information". First consider the extra information from the ocean response model. Our model only considers the passive response of the ocean to degree $\bar{n}$. This may be a reasonable approximation, because the ocean's response to higher-degree loading is monotonically decreasing, and at some point becomes insignificant. (This is ultimately a consequence of Newton's law of gravitation). In any case, the situation is better than the simpler assumption that mass exchange produces a uniform change in sea level [*Chao and O'Connor*, 1988].

[47] Second, extra information comes by assuming the land load is better characterized by equation (55) rather than a simple spherical harmonic expansion truncated to the same degree. This assumption is reasonable from the point of view that we do know that the land load is exactly zero except on land, and there will generally be a physically meaningful discontinuity in loading at the coastlines.

[48] Third, by truncating the underlying models at $\bar{n}$, we are implicitly assuming that all total load coefficients of degree higher than $\bar{n}$ are entirely driven by spectral leakage

from the lower-degree spherical harmonic forcing through the geographical distribution of continents and oceans. Whether or not this assumption is to be considered reasonable depends on a priori knowledge. For example, one working hypothesis might be that degree-2 seasonal mass redistribution is dominated by the interaction of degree-1 (i.e., interhemispheric) loading with the geographical distribution of the continents. One indicator to support this hypothesis is that VLBI baselines have annual signals with a geographic pattern of phase expected of a seasonal degree-1 signal, which is out of phase in opposite hemispheres [*Lavallée and Blewitt*, 2002].

5. Demonstration

5.1. Demonstration Goals

[49] We now demonstrate the above method on the simplest possible case, where we invert published seasonal degree-1 loading estimates from the GPS global network operated by the IGS. Apart from clarifying the steps of the calculation, the demonstration provides additional insight into the relationships between the various physical parameters, and the results provide an appreciation of the relative magnitudes of the various physical quantities discussed. Despite the obvious limitation in spatial resolution, it also provides quantitative first-order answers to several research questions. In the following demonstration, it should be kept in mind that although the solutions are constrained by physical self-consistency, they are entirely driven by observations of GPS surface deformation, with no a priori information on sea level or continental water. In effect, we are using the solid Earth itself as a weighing machine.

[50] The utility of this demonstration toward answering specific questions is naturally limited by the hemispheric-scale spatial resolution implied by degree-1 truncation. Interpretation of loading at a specific location would be suspect for continental water; however it would be more reasonable for the passive ocean response, due to its higher sensitivity to low-degree mass redistribution. The main goal of this exercise is to show how physical self-consistency governs the inversion procedure, and into the potential of this technique to investigate the global hydrological cycle. By its nature, the technique provides valuable integral constraints on the total load, which complements studies using specialized models. The resulting estimates of long-wavelength static ocean topography (and geoid deformation) might indicate to physical oceanographers the level of errors incurred when interpreting satellite altimeter data in terms of dynamic ocean topography.

5.2. GPS Data and Spectral Inversion for Earth's Shape

[51] We use the published empirical seasonal model of degree-1 deformation derived from a global GPS network [*Blewitt et al.*, 2001]. This in turn was derived from weekly estimates of the shape of the global network polyhedron over the period 1996.0–2001.0, provided by several IGS Analysis Centers using the fiducial-free method [*Heflin et al.*, 1992]. These were then combined by *Blewitt et al.* [2001] to produce station coordinate time series according to the method of *Davies and Blewitt* [2000] and *Lavallée* [2000]. Residual displacement time series were formed for each station by removing estimates of the velocity and initial position from the coordinate time series, taking care to reduce velocity bias by simultaneous estimation of annual and semiannual displacement signals [*Blewitt and Lavallée*, 2002]. The degree-1 deformation was then estimated every week, parameterized as a load moment vector in the CF frame. The load moment coordinate time series were then fit to an empirical seasonal model, parameterized by annual and semiannual amplitudes and phases.

[52] The load moment data need to be converted into equivalent height function data before we can start to apply our equations. To do this, we note that equation (14) is consistent with *Blewitt et al.* [2001, equation (6)] if we identify

$$\begin{pmatrix} H_{11}^C \\ H_{11}^S \\ H_{10}^C \end{pmatrix} = \frac{h_1'}{M_\oplus} \begin{pmatrix} m_x \\ m_y \\ m_z \end{pmatrix} \tag{58}$$

where h_1' is the height load Love number (CF frame) and $M_\oplus$ is the mass of the Earth. Table 4 shows the estimated degree-1 seasonal spectral coefficients for the height function, derived by equation (58) from the published load moment parameters of *Blewitt et al.* [2001]. *Blewitt et al.* [2001, Figure 2] show the height function and the gradient of the poloidal function (through their equation 11) explicitly at 2-monthly intervals using a stacking technique. The annual degree-1, order-0 (1,0) component dominates, associated with seasonal interhemispheric mass exchange, with maximum heights of 3 mm observed near the North Pole near the end of August and near the South Pole near the end of February.

[53] We scaled by a factor of 1.9 the one standard deviation formal errors of *Blewitt et al.* [2001], such that the chi-square per degree of freedom equals one when fitting the weekly degree-1 deformation solutions to the empirical seasonal model (D. Lavallée, personal communication, 2002). After this scaling, the errors in spectral amplitudes of height are at the level of 0.15 mm, which is a few percent of the (1,0) annual amplitude. While this appears to reflect formal error propagation and the empirical scatter in the data, it would not reflect interannual variability in the seasonal cycle, which subjectively appears to be at the 1-mm level. Therefore the computed errors might not accurately represent the errors in the seasonal model, however they should indicate the precision of the geodetic technique, and so suggest the potential of future analyses to resolve extra empirical parameters for better characterization of the time series.

5.3. Inversion for Total Load and Mean Relative Sea Level

[54] Season variation in the total load spectral coefficients was estimated using equation (31) and is shown in Table 4. The degree-0 term was set to zero to conserve mass. The total load follows the same spatial and temporal characteristics as the height function, but is opposite in sign (opposite in phase). Therefore the total load peaks near the North Pole near the end of February. The amplitude for the dominant

Table 4. Seasonal Degree-1 Inversion for Static Ocean Topography

Parameter	Annual		Semiannual	
	Amplitude, mm	Phase,[a] deg	Amplitude, mm	Phase,[a] deg
Height Function Spectral Coefficients from GPS Inversion[b]				
$\hat{H}^C_{10}$	2.97 ± 0.12	236 ± 2	0.67 ± 0.12	27 ± 10
$\hat{H}^C_{11}$	0.90 ± 0.15	266 ± 9	0.31 ± 0.15	249 ± 26
$\hat{H}^S_{11}$	1.30 ± 0.13	165 ± 6	0.27 ± 0.12	121 ± 25
Total Load Spectral Coefficients[c]				
$\hat{T}^C_{00}$	0.0 ± 0	-	0.0 ± 0	-
$\hat{T}^C_{10}$	59.4 ± 2.5	56 ± 2	13.5 ± 2.4	207 ± 10
$\hat{T}^C_{11}$	18.0 ± 3.0	86 ± 9	6.3 ± 2.9	69 ± 26
$\hat{T}^S_{11}$	26.1 ± 2.6	345 ± 6	5.4 ± 2.4	301 ± 25
Geocentric Sea Level and Geoid Height Spectral Coefficients[d]				
$\hat{N}^C_{00}$	0.0 ± 0	-	0.0 ± 0	-
$\widetilde{O}^C_{00} = \Delta V/g$	6.1 ± 0.3	234 ± 3	0.7 ± 0.3	20 ± 22
$\widetilde{O}^C_{10} = \hat{N}^C_{10}$	11.3 ± 0.5	56 ± 2	2.6 ± 0.5	207 ± 10
$\widetilde{O}^C_{11} = \hat{N}^C_{11}$	3.4 ± 0.6	86 ± 9	1.2 ± 0.6	69 ± 26
$\widetilde{O}^S_{11} = \hat{N}^S_{11}$	5.0 ± 0.5	345 ± 6	1.0 ± 0.5	301 ± 25
Relative Sea Level Quasi-Spectral Coefficients[e]				
$\widetilde{S}^C_{00} = \Delta V/g$	6.1 ± 0.3	234 ± 3	0.7 ± 0.3	20 ± 22
$\widetilde{S}^C_{10} = \widetilde{O}^C_{10} - \hat{H}^C_{10}$	14.3 ± 0.6	56 ± 2	3.2 ± 0.6	207 ± 10
$\widetilde{S}^C_{11} = \widetilde{O}^C_{11} - \hat{H}^C_{11}$	4.3 ± 0.7	86 ± 9	1.5 ± 0.7	69 ± 26
$\widetilde{S}^S_{11} = \widetilde{O}^S_{11} - \hat{H}^S_{11}$	6.3 ± 0.6	345 ± 6	1.3 ± 0.6	301 ± 25

[a]Uses the convention $\cos[2\pi f(t - t_0) - \phi_f]$, where f is frequency, t is time, t_0 is 1 January; so $\phi_f/2\pi f$ is time when f harmonic is maximum.

[b]Derived from equation (58) using data from 1996.0 to 2001.0 in center of figure frame [*Blewitt et al.*, 2001]. One standard deviation formal errors are scaled here by factor 1.9 to normalize the chi-square per degree of freedom for the seasonal model.

[c]Degree-0 total load constrained to zero due to conservation of mass. All other coefficients use surface height to load thickness ratio in Table 1.

[d]Degree-0 geocentric sea level computed by equation (45). All other coefficients use geoid height to load thickness ratio in Table 1.

[e]Can be computed equivalently using sea level to load thickness ratio in Table 1.

(1,0) spectral component is equivalent to a 59-mm column of seawater; at a later stage of the calculation we will be able to distinguish how much of this can be attributed spatially to loading on land versus the oceans.

[55] What we can calculate at this stage is the total amount of mass on land (which equals the negative amount of mass in the oceans), by integrating the total load over continental areas; thus we can calculate the contribution of mass exchange to mean relative sea level. Using equation (32), Table 5 shows our results for mean relative sea level, which has annual amplitude 8.0 ± 0.4 mm peaking toward the end of August. From equation (34), our result corresponds to ocean-continent mass exchange of annual amplitude $(2.92 \pm 0.14) \times 10^{15}$ kg, with continental mass peaking toward the end of February.

5.4. Inversion for Static Ocean Topography

[56] The sea surface follows the shape of the deformed geoid, thus geocentric sea level and the deformed geoid are identical for spectral components of degree 1 and above. Using equation (47) and tabulated "geoid height: load thickness" coefficients in Table 1, Table 4 shows our results for seasonal variation in the deformed geoid. The degree-0 geoid height is constrained to zero due to total mass conservation. The annual (1,0) term dominates with amplitude 11.3 ± 0.5 mm, peaking toward the end of August. The (1,1) terms are both less than half this amplitude.

[57] The degree-1 height of the geoid is reference-frame-dependent. Here it is reckoned with respect to the origin of the center of figure frame (CF). Thus the height of the degree-1 geoid is simply a consequence of "geocenter motion," defined as the motion of CF with respect to the center of mass of the entire Earth system (CM). In the CM frame, for example, there would be no degree-1 geoid height variation, and therefore no degree-1 component of geocentric sea level. However, satellite altimetry measurements are based on the derived coordinates of the satellite altimeter, which typically do not incorporate seasonal geocenter variations in the tracking station coordinates, and therefore relate more closely to CF than CM.

Table 5. Seasonal Inversion for Global Mean Oceanographic Parameters[a]

Parameter	Annual		Semiannual	
	Amplitude, mm	Phase, deg	Amplitude, mm	Phase, deg
Mean relative sea level $\overline{S}$[b]	8.0 ± 0.4	234 ± 3	1.0 ± 0.7	20 ± 22
Mean marine geoid height $\overline{N}$	1.5 ±0.1	234 ± 3	0.2 ± 0.1	20 ± 22
Mean ocean floor height $\overline{H}$	0.40 ± 0.02	54 ± 3	0.05 ± 0.02	200 ± 22
Mean geocentric sea level $= \overline{O} + \overline{S} + \overline{H}$	7.6 ± 0.4	234 ± 3	0.9 ± 0.4	20 ± 22
Sea surface geopotential height[c] $\Delta V/g = \overline{O} - \overline{N}$	6.1 ± 0.3	234 ± 3	0.7 ± 0.3	20 ± 22

[a]Mean values over oceanic areas computed in spectral domain using ocean function coefficients of Table 1.

[b]Mean relative sea level computed equivalently using either total load spectral coefficients or the quasi-spectral sea level coefficients.

[c]Above deformed geoid.

[58] However, degree-1 variation in relative sea level is not frame dependent, since it relates to the sea surface height above the deformed ocean floor rather than above a frame origin. Table 4 lists our solution for degree-1 quasi-spectral coefficients of relative sea level, computed as the difference between the heights of the deformed geoid height and the ocean floor, equation (42).

[59] Table 4 also shows the degree-0 coefficient for geocentric sea level computed as the geopotential height of sea level with respect to the deformed geoid, equation (45). This is identical to the degree-0 quasi-spectral relative sea level, because the global average change in height of the solid Earth surface is zero (due to mass conservation). The annual variation in geopotential height of the sea surface is 6.1 ± 0.3 mm, peaking near the end of August.

[60] This is by far the largest annual volumetric component of mean relative sea level (Table 5), the other two volumetric components being the mean marine geoid height with annual amplitude 1.5 ± 0.1 mm, and the mean height of the deformed ocean bottom with annual amplitude 0.40 ± 0.02 mm (of opposite phase). Added together appropriately, mean relative sea level has annual amplitude 8.0 ± 0.4 mm (consistent with our previous calculation using the total load); mean geocentric sea level (in the CF frame) has annual amplitude 7.6 ± 0.4 mm, equation (48), peaking on 25 August.

[61] Seasonal variations in sea level depend strongly on location (Figures 2 and 3), with seasonal peak values ranging from 3 to 19 mm. The smallest variations occur in the northern midlatitude Pacific; the annual signal can become so small that the semiannual signal dominates, which gives rise to two seasonal peak values as low as 3 mm in April and November. The largest variations occur in polar regions. Since the degree-0 quasi-spectral coefficient of relative sea level and the (1,0) coefficient are approximately six months out of phase, the geographic pattern of sea level is highly asymmetric between the Arctic and Antarctic (Figure 4). In the Arctic, these two terms interfere destructively, such that the seasonal variation in sea level peaks at approximately 9 mm in late March (including the semiannual terms). However, in the Antarctic, the two coefficients add constructively, such that the seasonal variation in sea level peaks at approximately 18 mm in mid-August. The intuitive reason for this is that, in the Arctic, the gravitational attraction of the large amount of water (retained on land in Northern Hemisphere winter) draws sea level higher, however this is partly cancelled by the global reduction in sea level necessary to provide mass balance. However, in the Antarctic, these two effects add together constructively. The underlying reason is that far more water is retained on land in the Northern Hemisphere than Southern Hemisphere in their respective winter seasons.

5.5. Inversion for Continental Water Topography

[62] Global spectral coefficients for relative sea level were computed from the quasi-spectral coefficients using the product-to-sum transformation, equation (52), where the transformation is given in Table 3. Results of this calculation up to degree 1 are shown in Table 6 (in principle, there are contributions from all degrees to infinity). This then enables calculation of the global spectral coefficients for continental water loading using equation (54). Because of mass conservation and as Table 6 shows, the degree-0 coefficient for the continental load, with annual amplitude 5.6 ± 0.3 mm peaking in late February, is of the same magnitude but opposite phase as the degree-0 coefficient of relative sea level.

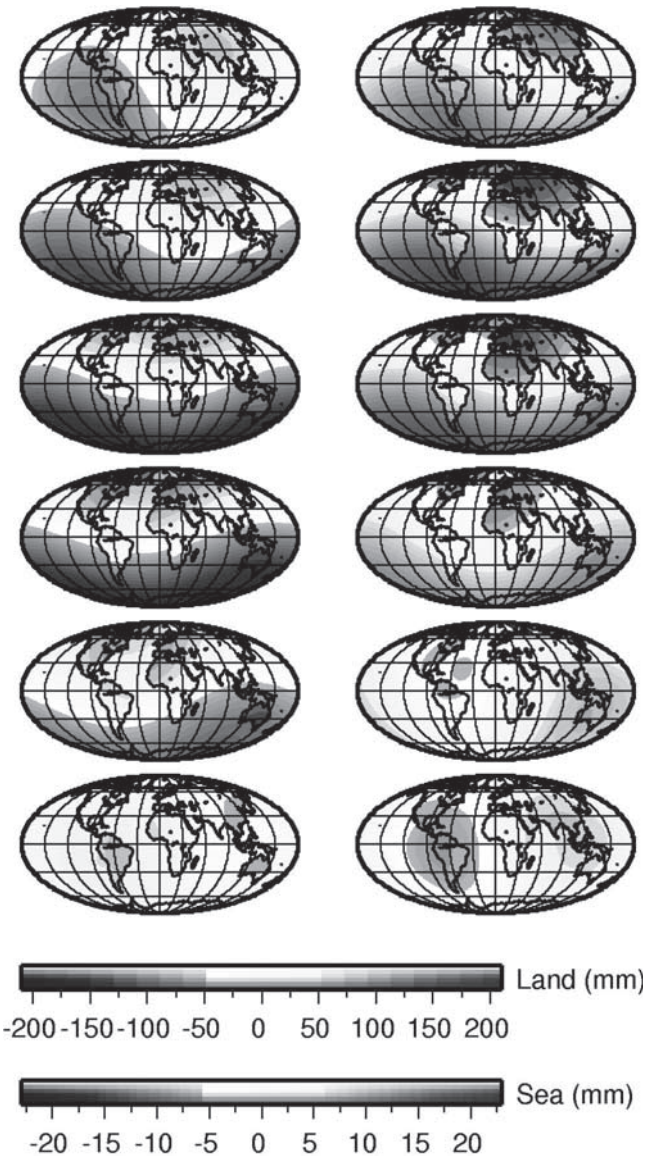

Figure 2. Monthly snapshots of mass distribution on land and in the oceans derived from observed degree-1 deformation: (left) (top to bottom) 1 January through 1 June, and (right) 1 July through 1 December. Different scales are used for land and ocean distributions, as there is a factor of 10 more load variation on land than in the oceans. See color version of this figure at back of this issue.

[63] The annual amplitudes for degree-1 continental loading are approximately 3–5 times larger for the land load than for the ocean load; the (1,0) coefficient dominates at 49.1 ± 2.1 mm, peaking in late February. This directly relates to the relative contribution of land loading and ocean loading to the total degree-1 load (and hence geocenter variations).

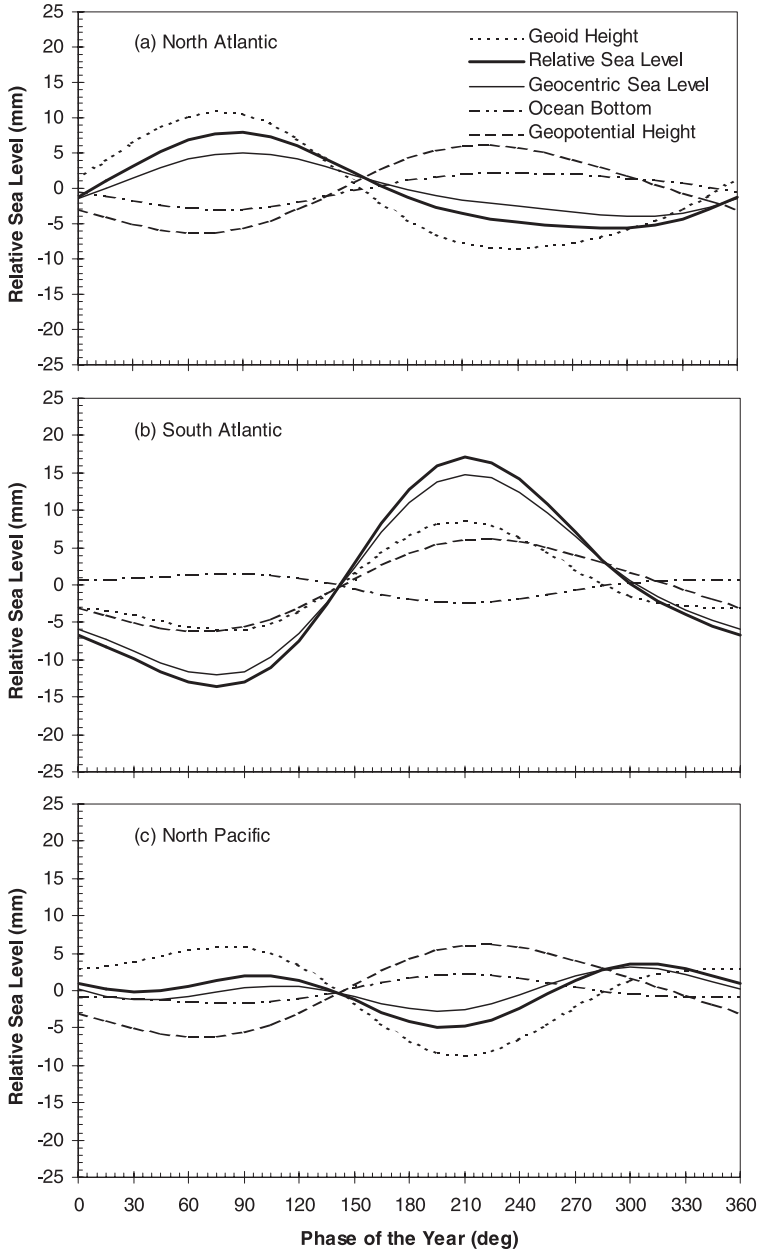

Figure 3. Seasonal variation in the constituents of sea level at three sample locations showing very different behavior: (a) North Atlantic (45°N, −30°E), where sea level variation is smaller than geoid variation due to less total oceanic water (which controls the sea surface geopotential) in Northern Hemisphere winter when gravitational attraction from land is largest; (b) South Atlantic (−45°N, −10°E), where geoid variation and oceanic water are in phase, causing larger variations in sea level; and (c) North Pacific (45°N, −170°E) where competing effects approximately cancel the annual variation, so semiannual variation dominates.

[64] Equation (56) was inverted using the inverse of the product-to-sum transformation (Table 3) truncated to degree 1. Table 6 shows the estimated quasi-spectral coefficients of the land load. Figure 2 also shows the spatial inversion for land load along with sea level. Figure 2 shows that the pattern of spatial variation in oceanic mass redistribution is similar to that on land, although it is approximately a factor of 10 smaller. The land load is dominated by the (1,0) annual coefficient, at 150.1 ± 6.4 mm, peaking at the end of February. However, the degree-0 coefficient is almost exactly out of phase with this (1,0) coefficient, such that it reduces the peak load in the Arctic Circle, but enhances it in the Antarctic. Intuitively, the reason for this out-of-phase behavior is related to the larger amount of land in the Northern Hemisphere and the need for the total land load to be a relatively small mass. Simply put, when the (1,0) term is large, it contributes a lot to mass on land. This is partly balanced by a

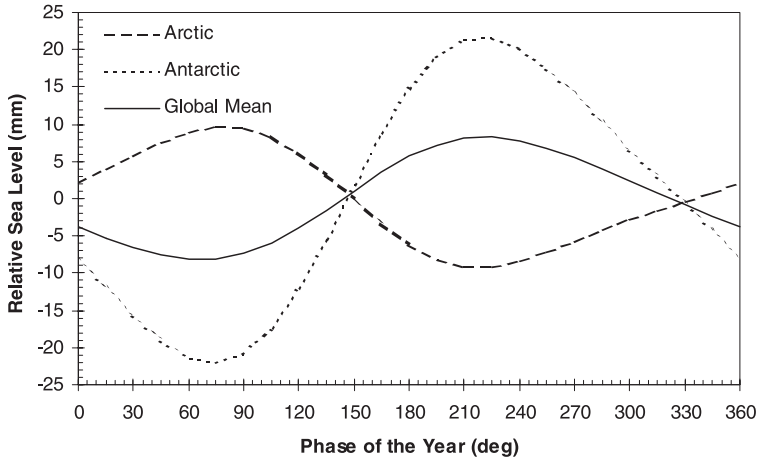

Figure 4. Seasonal variation in relative sea level compared between the Arctic (75°N, 0°E) and Antarctic (−75°N, 180°E). As would be expected for seasonal forcing, the phase is opposite between these locations. The difference in amplitude can be explained almost entirely by the annual variation in mean sea level, which in turn is caused by the asymmetry in continental area between the Northern and Southern Hemispheres.

degree-0 term of opposite phase such that the total land load is sufficiently small so that the landmass budget balances with mean relative sea level.

5.6. Discussion of Results

[65] As previously noted, the interpretation of the above results should be limited to spatial resolution of hemispheric scale. By comparing results with those from independent techniques, it would be useful to assess the extent to which a degree-1 truncated model can predict large-scale phenomena, such as seasonal variation in global mean sea level. First, consider our result on global mean geocentric sea level with annual amplitude 7.6 ± 0.4 mm with maximum sea level occurring on 25 August. This is to be compared (Figure 5) with annual amplitudes from TOPEX-Poseidon, which (after correction for steric effects) are in the range 7–10 mm, peaking during the period 12–24 September [*Chen et al.*, 1998, 2002; *Minster et al.*, 1999]. Assuming the large steric corrections (of order 5 mm in amplitude, half the total effect) are correct, this good agreement between our result and that of altimetric methods suggests that seasonal interhemispheric mass transfer is the dominant driving mechanism for seasonal change in sea level. In contrast, hydrological models of global mean sea level differ by up to a factor of 3; thus geodesy provides useful constraints on global hydrological models [*Chen et al.*, 2002].

[66] Our result on ocean-continent mass exchange of annual amplitude (2.92 ± 0.14) × 10^{15} kg, with continental mass peaking toward the end of February, implies a peak-to-peak seasonal continental mass variation of (5.8 ± 0.3) ×

Table 6. Seasonal Inversion for Continental Water Topography[a]

	Annual		Semiannual	
Parameter	Amplitude, mm	Phase, deg	Amplitude, mm	Phase, deg
	Relative Sea Level Global Spectral Coefficients[b] $\hat{S}(\Omega) = C(\Omega)\widetilde{S}(\Omega)$			
$\hat{S}^C_{00}$	5.6 ± 0.3	234 ± 3	0.7 ± 0.3	20 ± 22
$\hat{S}^C_{10}$	10.3 ± 0.4	57 ± 2	2.3 ± 0.4	206 ± 10
$\hat{S}^C_{11}$	3.9 ± 0.6	80 ± 9	1.1 ± 0.6	71 ± 29
$\hat{S}^S_{11}$	4.4 ± 0.4	345 ± 6	0.9 ± 0.4	305 ± 26
	Continental Water Global Spectral Coefficients[c]			
$\hat{L}^C_{00} = -\hat{S}^C_{00}$	5.6 ± 0.3	54 ± 3	0.7 ± 0.3	200 ± 22
$\hat{L}^C_{10} = \hat{T}^C_{10} - \hat{S}^C_{10}$	56 ± 2	11.2 ± 2.0	207 ± 10	
$\hat{L}^C_{11} = \hat{T}^C_{11} - \hat{S}^C_{11}$	14.2 ± 2.4	88 ± 10	5.2 ± 2.3	69 ± 26
$\hat{L}^S_{11} = \hat{T}^S_{11} - \hat{S}^S_{11}$	345 ± 6	4.5 ± 2.0	300 ± 26	
	Continental Water Quasi-Spectral Coefficients[d] $\hat{L}(\Omega) = [1 - C(\Omega)]\widetilde{L}(\Omega)$			
$\widetilde{L}^C_{00}$	30.1 ± 2.0	238 ± 4	2.3 ± 1.9	345 ± 18
$\widetilde{L}^C_{10}$	150.1 ± 6.4	58 ± 2	34.7 ± 6.1	205 ± 10
$\widetilde{L}^C_{11}$	61.2 ± 11.2	85 ± 10	24.1 ± 10.9	65 ± 26
$\widetilde{L}^S_{11}$	68.5 ± 7.2	337 ± 6	15.1 ± 6.8	316 ± 26

[a]Errors propagated formally without a priori uncertainty on total load coefficients of degree 2 and higher (which may have spectral leakage).

[b]Computed in the spectral domain by product-to-sum transformation (Table 3) according to equation (52). Full spectrum exists in principle.

[c]Given to the degree to which total load has been estimated (degree 1).

[d]Computed using inverse of product-to-sum matrix truncated at degree 1.

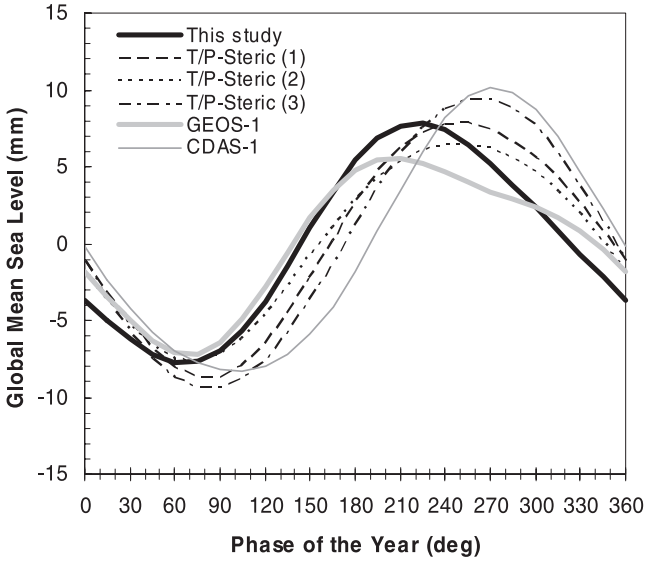

Figure 5. Seasonal variation in geocentric global mean sea level, comparing the results of this study to those derived from TOPEX-Poseidon data minus a steric model: (1) *Chen et al.* [2002], (2) *Chen et al.* [1998], and (3) *Minster et al.* [1999]. Our geocentric results are with respect to the center of figure (CF) frame [*Blewitt*, 2003]. Also shown for comparison are two hydrological predictions of relative global mean sea level calculated from the NCAR CDAS-1 model [*Chen et al.*, 2002] and the NASA GEOS-1 model [*Chen et al.*, 1998], although other hydrological predictions not shown here can differ in amplitude by a factor of 3 [*Chen et al.*, 2002].

10^{15} kg. By comparison, satellite radar altimetry (of the surface and base) of the Northern Hemisphere snowpack have been used to infer a peak-to-peak snow mass of 3×10^{15} kg [*Chao et al.*, 1987; *Chang et al.*, 1990] peaking during February–March. Taken together with our result, this constrains the planet's peak-to-peak seasonal groundwater mass to be $<3 \times 10^{15}$ kg (excluding snow), assuming it has a similar phase. This is consistent with (but stronger than) the order-of-magnitude analysis of *Blewitt et al.* [2001], which set an upper bound to winter groundwater at $<7 \times 10^{15}$ kg. Even stronger upper bounds are possible if we assume an out of phase contribution to the total mass exchange from seasonal snowpack variations in Antarctica (which was not included in the satellite radar results).

[67] Note in Figure 5 the asymmetric shape of our estimate of seasonal variation in global mean sea level. The maximum slope is 63% greater than the magnitude of the minimum slope. A similar asymmetry is also seen in the TOPEX-Poseidon results and in the hydrological models. This strongly indicates that water runoff in Northern Hemisphere spring [*Dai and Trenberth*, 2002] takes place at a much faster rate than continental water accumulation toward the end of the year.

[68] While we have shown results of our inversion on seasonal variation in sea level at specific geographic locations, it would be difficult to make a meaningful comparison with other techniques, because of the large uncertainty in the ocean's dynamic topography. However, one clear conclusion from our results is that physical self-consistency forces the ocean to have seasonal static topography at the level of 10 mm. As a rule of thumb, sea level variations in offshore regions appeared to be ~10% of the water-equivalent height of the adjacent continental load. Table 7 shows that the passive ocean response to degree-1 loading amplifies the annual degree-1 land load by 21–27%, but that the ocean does not change the annual phase significantly (~1 day). This is in intuitive accord with the above rule of thumb if we multiply 10% by the ratio of ocean to land areas. We deduce that models of solid Earth deformation on the global scale (typically using Green's functions) and models of geocenter displacements, based on adding together contributions from the land and oceans, may be biased at this level unless self-consistency is rigorously incorporated.

Table 7. Amplification of Degree-1 Loading by Passive Ocean Response

Parameter Comparison	Annual		Semiannual	
	Amplitude Ratio[a]	Phase Shift,[b] deg	Amplitude Ratio[a]	Phase Shift,[b] deg
$\hat{T}^C_{10}$ relative to $\hat{L}^C_{10}$	1.21	0.1	1.20	−0.2
$\hat{T}^C_{11}$ relative to $\hat{L}^C_{11}$	1.27	−1.6	1.22	0.4
$\hat{T}^S_{11}$ relative to $\hat{L}^S_{11}$	1.20	0.1	1.20	0.7

[a]Defined as the ratio of spectral amplitudes of the total (continental plus ocean) load to the continental load.
[b]Defined as the difference in phase between the total load and continental load.

[69] Our spatial inversion for sea level indicates that attention should be paid to the asymmetry in ocean bottom pressure in the Arctic versus Antarctic. The demonstration showed how this is a consequence of a larger seasonal variation in water retained on land in the Northern Hemisphere versus the Southern Hemisphere (thus the geoid height is of opposite phase to global mean sea level in the Arctic, and of similar phase in the Antarctic).

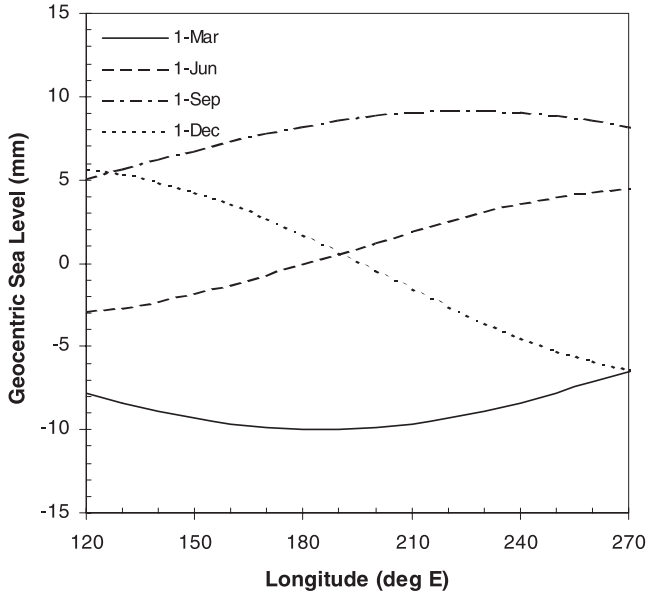

Figure 6. Snapshots of the longitudinal profile in equatorial sea level across the Pacific Ocean, showing a seasonal "see-saw" effect.

Table 8. Reconstruction of Total Load and Height Function[a]

Parameter	Annual Amplitude, mm	Annual Phase, deg	Semiannual Amplitude, mm	Semiannual Phase, deg
	Consistency Check, Degree-1 Total Load[b]			
$\hat{T}^C_{00}$	0.0 ± 0	–	0.0 ± 0	–
$\hat{T}^C_{10}$	59.4 ± 2.5	56 ± 2	13.5 ± 2.4	207 ± 10
$\hat{T}^C_{11}$	18.0 ± 3.0	86 ± 9	6.3 ± 2.9	69 ± 26
$\hat{T}^S_{11}$	26.1 ± 2.6	345 ± 6	5.4 ± 2.4	301 ± 26
	Predicted Degree-2 Total Load[c]			
$\hat{T}^C_{20}$	5.1 ± 1.4	28 ± 16	4.9 ± 1.3	225 ± 16
$\hat{T}^C_{21}$	6.9 ± 0.6[d]	48 ± 5	0.2 ± 0.6	79 ± 148
$\hat{T}^S_{21}$	11.0 ± 0.9[d]	22 ± 5	1.1 ± 0.9	286 ± 46
$\hat{T}^C_{22}$	0.5 ± 0.5	88 ± 5	1.3 ± 0.5	44 ± 20
$\hat{T}^S_{22}$	5.3 ± 0.5	50 ± 5	0.3 ± 0.5	76 ± 102
	Predicted Degree-2 Height Function[c]			
$\hat{H}^C_{20}$	0.57 ± 0.15	208 ± 16	0.55 ± 0.15	45 ± 16
$\hat{H}^C_{21}$	0.77 ± 0.07[d]	228 ± 5	0.03 ± 0.07	259 ± 148
$\hat{H}^S_{21}$	1.23 ± 0.10[d]	202 ± 5	0.12 ± 0.10	106 ± 46
$\hat{H}^C_{22}$	0.05 ± 0.05	268 ± 5	0.15 ± 0.05	224 ± 20
$\hat{H}^C_{22}$	0.60 ± 0.05	230 ± 5	0.03 ± 0.05	256 ± 102

[a]Computed only using estimates and full covariance matrix of quasi-spectral coefficients (to degree 1) for relative sea level and continental water by applying equation (57) up to degree 2.

[b]Coefficients to degree 1 should (and do) agree with initial values in Table 3.

[c]Degree-2 predictions only represent the contribution of loading given quasi-spectrally to degree 1, by its spectral interaction with the ocean function. Actual degree-2 load will also include higher quasi-spectral degree loading, which may contribute constructively or destructively.

[d]Seasonal degree-1 annual loading interacting with the ocean function leaks strongly into annual degree-2, order-1 terms, indicating a potential mechanism to excite the Chandler wobble.

[70] The potential of this technique is perhaps best illustrated by the spatial inversion's prediction on long-wavelength seasonal gradients in static ocean topography (both relative and geocentric). For example, our solution predicts a 10 mm east-west sea surface height difference spanning the equatorial Pacific Ocean (15,000 km) which behaves like an annual see-saw (Figure 6). The largest see-saw gradients are observed in the equatorial Pacific and Atlantic Ocean in the north-south direction where, at their seasonal peak, sea level can vary 20 mm over 10,000 km. We caution that such gradients in static topography might be misinterpreted in terms of basin-scale dynamics when analyzing satellite altimeter data.

6. Prospects for Higher Resolution Inversion

6.1. Reconstruction of Total Load and Height Function to Degree 2

[71] We speculate on prospects for positive identification and interpretation of seasonal signals at higher degrees. Let us first consider degree-2 loading. Using equation (57), Table 8 shows the degree-2 coefficients of the total load, assuming that relative sea level and the continental water load have no significant quasi-spectral power above degree 1. We call this the "degree-1 dominance hypothesis," and offer no evidence at this stage that it holds, except to conjecture that seasonal retention of water on land might be dominated by mass exchange between the Northern and Southern Hemispheres. While this hypothesis has more general implications, our purpose here is to quantify the magnitude of possible degree-2 signals and thus assess the feasibility of detection. The solution predicts that degree-2 load would be dominated by the T^S_{21} amplitude of 11.0 ± 0.9 mm (peaking in late January).

[72] The results of Table 8 reflect the contribution to degree-2 loading from the interaction of a degree-1 pattern of continental water masked by the geographic distribution of the continents. This could lend insight into possible mechanisms for polar motion excitation by (2,1) coefficients. In particular, we suggest the annual (2,1) coefficient as a plausible mechanism to excite the Chandler wobble, if sufficiently large.

[73] The contribution of degree-1 land loading to degree-2 surface height deformation is largest in the annual coefficients at H^C_{21} = 0.77 ± 0.07 mm and H^S_{21} = 1.23 ± 0.10 mm, both peaking in the late July to mid-August time frame. Judging by the clear detection of degree-1 height signals of similar magnitude, the annual (2,1) coefficients should be at detectable levels. The magnitude of the predicted degree-2 signals is partly due to the fact that, of all the degrees, degree-2 deformation has the largest surface height to load thickness ratio at 11.2% (Table 1), which is more than twice that of degree-1 in the CF frame at 5%. We conclude that degree-1 land loading alone should be sufficient to create a detectable degree-2 deformation signal.

6.2. Higher Degrees

[74] Signal detection of higher degrees depends on three things. First, as previously discussed, is the issue of the number and distribution of GPS stations, which in principle might currently limit detection to around degree-9.

[75] Second, there must be sufficient power in the actual loads at higher degrees. Loading models predict significant variation in hydrologic loading (at the several millimeter deformation level) on continental scales [*Van Dam et al.*, 2001], so this would not appear to be a limiting factor, assuming that the goal is inversion in the spatial domain.

[76] Thirdly, there must be a sufficient deformation response of the solid Earth at higher degrees as compared measurement errors. As Table 1 shows, beyond degree 2 the surface height to load thickness ratio decreases monotonically. By degree 9 the ratio has fallen to 4%. This is of similar magnitude to degree 1, which is clearly detectable.

[77] The evidence therefore suggests that spectral inversion of loading up to degree 9 and spatial inversion of continental-scale loads are feasible. It is recommended that covariance analysis be used (in parallel with attempts to interpret deformation data) to understand how the estimated spectral coefficients are theoretically correlated for the global IGS network, and how this maps into spatial resolution.

7. Conclusions

[78] We have developed an inversion method for mass redistribution on the Earth's surface given GPS measurements of the solid Earth's varying geometrical shape. The method is based on a load Love number formalism, using gravitational self-consistency to infer the relative contribu-

tions of relative sea level and continental water loading to the estimated spectral coefficients of the total load responsible for the observed deformation. The method was demonstrated for the simplest possible case using published seasonal degree-1 deformations from the global IGS network [*Blewitt et al.*, 2001]. Inversion produces results on relative mean sea level in terms of the geoid height, the geopotential height of the sea surface (above the geoid), and the height of the deformed ocean bottom. The demonstration illustrates how the relative contribution of the various constituents of sea level is dependent on time of year and geographic location.

[79] We find the annual amplitude of ocean-continent mass exchange is $(2.92 \pm 0.14) \times 10^{15}$ kg with maximum ocean mass on 25 ± 3 August, corresponding to annual amplitudes for mean relative sea level at 8.0 ± 0.4 mm, and for mean geocentric sea level at 7.6 ± 0.4 mm. This result confirms results from TOPEX-Poseidon (after steric correction), and places strong constraints on physically acceptable hydrological models (which can differ by factors of three). It also confirms that the steric corrections applied to TOPEX-Poseidon data are reasonable as a global average. Taking into account satellite altimeter measurements of the Northern Hemisphere snowpack (at 3×10^{15} kg, peak to peak), our results strongly constrain global groundwater to have a peak-to-peak seasonal variation $<3 \times 10^{15}$ kg.

[80] The seasonal variation in sea level at a point strongly depends on location, with typical amplitudes of 10 mm, the largest being ~20 mm around Antarctica in mid-August. Sea level variations are predicted to be smaller in the Northern Hemisphere due to the hemispheric asymmetry in continental area. Sea level is lowered everywhere to provide continental water in the Northern Hemisphere winter, but at the same time this continental water raises sea level in the Northern Hemisphere through gravitational attraction. Seasonal gradients in static topography have amplitudes of up to 10 mm over 5,000 km, which may be misinterpreted as dynamic topography. Peak continental loads are predicted to occur in polar regions in mid-winter at the water-equivalent level of 100–200 mm.

[81] An analysis of the potential for this method to estimate the seasonal surface load with higher spatial resolution indicates that estimation to degree 9 is feasible. This should allow for spatial resolution of continental-scale hydrology. Finally, we have developed a general scheme (Figure 1), which shows the potential for connecting various geodetic data types through models of the globally loaded Earth system. For example, it should be possible to jointly invert GPS station position time series with independent data on seasonal variation in the Earth's gravity field up to degree and order 4, now available from satellite laser ranging [*Nerem et al.*, 2000], with potentially much higher spatial resolution predicted from missions like GRACE [*Wahr et al.*, 1998].

Appendix A: Spherical Harmonics Convention

[82] Recognizing "errors which arose from normalization conventions" in the literature [*Chao and O'Connor*, 1988], we choose to use classical, real-valued, unnormalized spherical harmonics with the phase convention according to *Lambeck* [1988]. An arbitrary function $f(\Omega)$ defined on a spherical surface as function of position Ω (latitude φ, longitude λ) can be expanded as

$$f(\Omega) = \sum_{n=0}^{\infty} \sum_{m=0}^{n} \sum_{\Phi}^{\{C,S\}} f_{nm}^{\Phi} Y_{nm}^{\Phi}(\Omega) = \sum_{n=0}^{\infty} \left[f_{00}^{C} Y_{00}^{C}(\Omega) + \sum_{m=1}^{n} \left(f_{nm}^{C} Y_{nm}^{C}(\Omega) + f_{nm}^{S} Y_{nm}^{S}(\Omega) \right) \right] \quad \text{(A1)}$$

where the cosine ($\Phi = C$) and sine ($\Phi = S$) spherical harmonic basis functions are defined by

$$Y_{nm}^{C}(\Omega) = P_{nm}(\sin\varphi)\cos m\lambda \qquad Y_{nm}^{S}(\Omega) = P_{nm}(\sin\varphi)\sin m\lambda \quad \text{(A2)}$$

and where the associated Legendre polynomials are

$$P_{nm}(x) = \left[\left(1 - x^2\right)^{m/2} / 2^n n! \right] \left(d^{n+m}/dx^{n+m} \right) \left(x^2 - 1\right)^n \quad \text{(A3)}$$

The integral of two spherical harmonics is

$$\oiint Y_{nm}^{\Phi}(\Omega) Y_{n'm'}^{\Phi'}(\Omega) d\Omega = \delta_{nn'} \delta_{mm'} \delta_{\Phi\Phi'} \frac{4\pi}{\Pi_{nm}^2} \quad \text{(A4)}$$

where $d\Omega = d(\sin\varphi) d\lambda$ and

$$\Pi_{nm} = \left[(2 - \delta_{m0})(2n+1) \frac{(n-m)!}{(n+m)!} \right]^{\frac{1}{2}} \quad \text{(A5)}$$

The spherical harmonic coefficients in equation (A1) are therefore

$$f_{nm}^{\Phi} = \frac{\Pi_{nm}^2}{4\pi} \oiint f(\Omega) Y_{nm}^{\Phi} d\Omega \quad \text{(A6)}$$

It is to be understood that Y_{n0}^{S} and f_{n0}^{S} are to be excluded from all equations.

Appendix B: Product-to-Sum Conversion: Recursive Method for Real Spherical Harmonics

[83] According to equation (52), the ocean function product-to-sum conversion formula can be written in coefficient form

$$\left[C(\Omega) \widetilde{S}(\Omega) \right]_{nm}^{\Phi} = \sum_{n'm'\Phi'} \left[\sum_{n''m''\Phi''} A_{nm,n'm',n''m''}^{\Phi,\Phi',\Phi''} C_{n''m''}^{\Phi''} \right] \widetilde{S}_{n'm'}^{\Phi'} \quad \text{(B1)}$$

where $\widetilde{S}(\Omega)$ is the smooth sea level function, and $C(\Omega)$ is the ocean function defined to be 1 over the oceans and 0 on land. The notation for spherical harmonic coefficients is given in Appendix A. Evaluation of equation (B1) first requires a general solution to the following integral of triple real-valued spherical harmonics defined by equation (50):

$$A_{nm,n'm',n''m''}^{\Phi,\Phi',\Phi''} = \frac{\Pi_{nm}^2}{4\pi} \oiint Y_{nm}^{\Phi}(\Omega) Y_{n'm'}^{\Phi'}(\Omega) Y_{n''m''}^{\Phi''}(\Omega) d\Omega \quad \text{(B2)}$$

Typically this integral is discussed in quantum mechanics for the case of complex spherical harmonics. For real-valued spherical harmonics, the integral over longitude is different, and there are no negative values of m.

[84] First of all, starting with the integral over latitude, our method uses recursion formulae for associated Legendre polynomials to derive recursion formulae for the integrals themselves. The following "selection rules" indicate which combinations of associated Legendre polynomials result in a nonzero integral over latitude:

$$\begin{gathered} m'' = |m \pm m'| \\ \max(|n - n'|, |m' \pm m''|) \le n'' \le n + n' \\ n + n' + n'' = 2p \end{gathered} \tag{B3}$$

where p is an integer. Let us define the integral over latitude for those indices that satisfy the above selection rules:

$$Q^{\pm}_{nm;n'm';n''} = \int_{-1}^{1} P_{nm}(x) P_{n'm'}(x) P_{n''|m\pm m'|}(x)\, dx \tag{B4}$$

The solution to this can always be constructed from the following general expression

$$Q^{+}_{n_1 m_1, n_2 m_2, n_3} \equiv \int_{-1}^{1} P_{n_1 m_1}(x) P_{n_2 m_2}(x) P_{n_3 (m_1 + m_2)}(x)\, dx \tag{B5}$$

which can then always be related to equation (B4) using the following identities derivable from equation (B5)

$$Q^{-}_{n_1 m_1; n_2 m_2; n_3} = \begin{cases} Q^{+}_{n_3 m_3; n_2 m_2; n_1} & \text{if } m_1 \ge m_2, (m_3 = m_1 - m_2) \\ Q^{+}_{n_3 m_3; n_1 m_1; n_2} & \text{if } m_2 \ge m_1, (m_3 = m_2 - m_1) \end{cases} \tag{B6}$$

Balmino [1978] presents a method to solve equation (B4) by decomposition of associated Legendre polynomials as an explicit function of their arguments. For computational efficiency, and to facilitate control on rationalization of fractions to mitigate potential overflow problems, we computed and tabulated results for (B5) using recursion relations for the integrals, which can be derived using recursion relations for associated Legendre polynomials [*Rikitake et al.*, 1987]. This is a somewhat simpler (but equivalent) method than suggested by *Balmino* [1978, 1994]. The recursion algorithm is now summarized. Starting with formulae for order zero, we have

$$\begin{aligned} Q^{+}_{n_1 0; n_2 0; 0} &= \frac{2\delta_{n_1 n_2}}{2n_1 + 1} \\ Q^{+}_{n_1 0; n_2 0; 1} &= \frac{2n_1 \delta_{n_1 n_2 + 1}}{(2n_1 - 1)(2n_1 + 1)} + \frac{2(n_1 + 1)\delta_{n_1 n_2 - 1}}{(2n_1 + 1)(2n_2 + 3)} \\ Q^{+}_{n_1 0; n_2 0; n_3} &= \frac{2n_3 - 1}{n_3 (2n_2 + 1)} \\ &\quad \cdot \left[(n_2 + 1) \cdot Q^{+}_{n_1 0; n_2 + 1, 0; n_3 + 1} + n_2 Q^{+}_{n_1 0; n_2 - 1, 0; n_3 - 1} \right] \\ &\quad - \frac{n_3 - 1}{n_3} Q^{+}_{n_1 0; n_2, 0; n_3 - 2} \end{aligned} \tag{B7}$$

from which we can then apply

$$\begin{aligned} Q^{+}_{n_1 1; n_2 0; n_3} &= \frac{Q^{+}_{n_1 0; n_2 0; n_3}}{2} \left[(n_1 - n_2)(n_1 + n_2 + 1) + n_3 (n_3 + 1) \right] \\ Q^{+}_{n_1 0; n_2 1; n_3} &= \frac{Q^{+}_{n_1 0; n_2 0; n_3}}{2} \left[-(n_1 - n_2) \cdot (n_1 + n_2 + 1) + n_3 (n_3 + 1) \right] \end{aligned} \tag{B8}$$

and then, finally, we can recursively compute

$$\begin{aligned} Q^{+}_{n_1 m_1; n_2 m_2; n_3} &= (n_1 + m_1)(n_1 - m_1 + 1) Q^{+}_{n_1 m_1 - 1; n_2 m_2; n_3} \\ &\quad + (n_2 + m_2)(n_2 - m_2 + 1) Q^{+}_{n_1 m_1; n_2 m_2 - 1; n_3} \\ Q^{+}_{n_1 m_1; n_2 m_2 + 1; n_3} &= (n_3 - m_1 - m_2)(n_3 + m_1 + m_2 + 1) Q^{+}_{n_1 m_1; n_2 m_2; n_3} \\ &\quad - Q^{+}_{n_1 m_1 + 1; n_2 m_2; n_3} \end{aligned} \tag{B9}$$

Note that there are generally many possible pathways to compute a specific coefficient. This is useful for self-consistency testing when tabulating the results.

[85] Equivalently, it can be shown that equation (B5) can be computed directly by

$$\begin{aligned} Q^{+}_{n_1 m_1, n_2 m_2, n_3} &= \frac{2}{2n_3 + 1} \sqrt{\frac{(n_1 + m_1)!(n_2 + m_2)!(n_3 + m_1 + m_2)!}{(n_1 - m_1)!(n_2 - m_2)!(n_3 - m_1 - m_2)!}} \\ &\quad \cdot \langle n_1, m_1; n_2, m_2 | n_3, m_1 + m_2 \rangle \langle n_1, 0; n_2, 0 | n_3, 0 \rangle \end{aligned} \tag{B10}$$

where $\langle n_1, m_1; n_2, m_2, | n_3, m_1 + m_2 \rangle$ is a Clebsch-Gordan coefficient, representing a unitary transformation between coupled and uncoupled basis states in quantum angular momentum theory. Clebsch-Gordan coefficients can be calculated according to the Racah formula [*Messiah*, 1963] and are tabulated and widely distributed in the particle physics community [*Particle Data Group*, 2002], thus making computer programs easier to verify.

[86] Now we must compute the integral over longitude. This vanishes unless the triple product of cosine and sine functions involves an odd number of cosines (understanding that zero-order sine functions are disallowed). Therefore $\Phi_3 = F(\Phi_1, \Phi_2)$ is uniquely determined. For these nonzero combinations, it can be shown that the longitude integral:

$$\begin{aligned} \Lambda^{\Phi_1 \Phi_2}_{m_1 m_2} &= \frac{1}{4\pi} \int_0^{2\pi} \begin{Bmatrix} \sin m_1 \lambda \\ \cos m_1 \lambda \end{Bmatrix}^{\Phi_1} \begin{Bmatrix} \sin m_2 \lambda \\ \cos m_2 \lambda \end{Bmatrix}^{\Phi_2} \\ &\quad \cdot \begin{Bmatrix} \sin(m_1 + m_2)\lambda \\ \cos(m_1 + m_2)\lambda \end{Bmatrix}^{F(\Phi_1, \Phi_2)} d\lambda \\ &= \frac{a(\Phi_1, \Phi_2)}{2(2 - \delta_{m_1 0})(2 - \delta_{m_2 0})} \end{aligned} \tag{B11}$$

where

$$\begin{aligned} F(\Phi_1, \Phi_2) &= \begin{cases} C & \text{if } \Phi_1 = \Phi_2 \\ S & \text{otherwise} \end{cases} \\ a(\Phi_1, \Phi_2) &= \begin{cases} -1 & \text{if } \Phi_1 = \Phi_2 = S \\ +1 & \text{otherwise} \end{cases} \end{aligned} \tag{B12}$$

According to identity (B6), we use can use the following selection rules in equation (B5) to compute all allowed

values of the Q coefficients:

$$(m_1, m_2, m_3) = \begin{cases} (m, m', m'') \text{if } m'' = m + m' \\ (m'', m', m) \text{if } m'' = m - m' \\ (m'', m, m') \text{if } m'' = m' - m \end{cases} \quad \text{(B13)}$$

and thus compute equation (B4) for any combination of $m'' = |m \pm m'|$. Using all the above tools, the ocean function product-to-sum coefficients in equation (B1) can be simplified using:

$$\sum_{n''=0}^{\infty} \sum_{m''=0}^{n''} \sum_{\Phi''}^{\{C,S\}} A^{\Phi,\Phi',\Phi''}_{nm,n'm',n''m''} C^{\Phi''}_{n''m''}$$

$$= \sum_{\substack{n''=\max(|n-n'|,m+m') \\ \text{if } n+n'+n''=\text{even}}}^{n+n'} \Pi^2_{nm} \Lambda^{\Phi\Phi'}_{mm'} Q^{+}_{nm;n'm';n''} C^{F(\Phi,\Phi')}_{n'',m+m'}$$

$$+ \sum_{\substack{n''=\max(|n-n'|,|m-m'|) \\ \text{if } n+n'+n''=\text{even}}}^{n+n'} \left\{ \begin{array}{ll} \Pi^2_{nm} \Lambda^{F(\Phi,\Phi')\Phi'}_{m',m-m'} Q^{+}_{n'',m-m';n'm';n} C^{F(\Phi,\Phi')}_{n'',m-m'} & \text{if } m \geq m' \\ \Pi^2_{nm} \Lambda^{F(\Phi,\Phi')\Phi}_{m'-m,m} Q^{+}_{n'',m'-m;nm;n'} C^{F(\Phi,\Phi')}_{n'',m'-m} & \text{if } m' \geq m \end{array} \right\} \quad \text{(B14)}$$

[87] The numerators and denominators are pure integers (as can be seen by inspection of the above formulae); so if they are computed separately, the answer can be represented as an exact rational fraction until the final step. At each step in the recursion the numerator and denominator are divided by their greatest common denominator, which can be important to prevent computational problems. (Even doing so, the number of digits required to represent the rational fraction grows quickly, as large as 11 digits for degree-3 theory, and so at some point floating-point calculations become necessary).

[88] Our recursive method was amenable to implementation in a spreadsheet, and the results (for low degree) are shown in Appendix C. We successfully verified the answers for low-degree expansions using published values of Clebsch-Gordan coefficients and complex spherical harmonics, which were then converted into results for real-valued spherical harmonics. This was all done by painstaking hand derivation so as to recover the rational fractions exactly in terms of integer numerators and denominators. Finally, we performed a second independent check by writing a FORTRAN program to tabulate the results of equation (B14) by applying the method of (B10) using a Clebsch-Gordan subroutine. Since this program has been validated, due to obvious advantages of speed and accurate bookkeeping, it will be employed for future higher-degree calculations.

Appendix C: Product-to-Sum Conversion: Results for Low Degrees

[89] We provide sample results of equations (52) and (B1) here as a benchmark to assist those attempting to apply our method. Consider the smooth sea level function $\tilde{S}(\Omega)$ that is defined globally as a spherical harmonic expansion, but is then projected onto the area covered by the ocean such that the result is exactly $\tilde{S}(\Omega)$ on the ocean, but zero on land. The spherical harmonic coefficients of the ocean-projected function are given by

$$\left[C(\Omega)\widetilde{S}(\Omega)\right]^{\Phi}_{nm} = \sum_{n'm'\Phi'} \left[\sum_{n''m''\Phi''} A^{\Phi,\Phi',\Phi''}_{nm,n'm',n''m''} C^{\Phi''}_{n''m''} \right] \widetilde{S}^{\Phi'}_{n'm'} \quad \text{(C1)}$$

Consider that $\tilde{S}(\Omega)$ is given exactly as a degree-2 spherical harmonic expansion. Note that in this case, only ocean function coefficients up to degree 4 are required for exact results. Results are now systematically provided for the projected function up to degree 2 using the method of Appendix B.

[90] Starting with degree 0 of the projected function we have

$$\left[C(\Omega)\widetilde{S}(\Omega)\right]^{C}_{00} = C^C_{00}\widetilde{S}^C_{00} + \frac{1}{3}C^C_{10}\widetilde{S}^C_{10} + \frac{1}{3}C^C_{11}\widetilde{S}^C_{11} + \frac{1}{3}C^S_{11}\widetilde{S}^S_{11} + \frac{1}{5}C^C_{20}\widetilde{S}^C_{20} + \frac{3}{5}C^C_{21}\widetilde{S}^C_{21} + \frac{3}{5}C^S_{21}\widetilde{S}^S_{21} + \frac{12}{5}C^C_{22}\widetilde{S}^C_{22} + \frac{12}{5}C^S_{22}\widetilde{S}^S_{22} \quad \text{(C2)}$$

For degree 1 we have

$$\left[C(\Omega)\widetilde{S}(\Omega)\right]^{C}_{10} = C^C_{10}\widetilde{S}^C_{00} + \left(C^C_{00} + \frac{2}{5}C^C_{20}\right)\widetilde{S}^C_{10} + \frac{3}{5}C^C_{21}\widetilde{S}^C_{11} + \frac{3}{5}C^S_{21}\widetilde{S}^S_{11} + \left(\frac{2}{5}C^C_{10} + \frac{9}{35}C^C_{30}\right)\widetilde{S}^C_{20} + \left(\frac{3}{5}C^C_{11} + \frac{36}{35}C^C_{31}\right)\widetilde{S}^C_{21} + \left(\frac{3}{5}C^S_{11} + \frac{36}{35}C^C_{31}\right)\widetilde{S}^S_{21} + \frac{36}{7}C^C_{32}\widetilde{S}^C_{22} + \frac{36}{7}C^S_{32}\widetilde{S}^S_{22} \quad \text{(C3)}$$

$$\left[C(\Omega)\widetilde{S}(\Omega)\right]^{C}_{11} = C^C_{11}\widetilde{S}^C_{00} + \frac{3}{5}C^C_{21}\widetilde{S}^C_{10} + \left(C^C_{00} - \frac{1}{5}C^C_{20} + \frac{6}{5}C^C_{22}\right)\widetilde{S}^C_{11} + \frac{6}{5}C^S_{22}\widetilde{S}^S_{11} + \left(-\frac{1}{5}C^C_{11} + \frac{18}{35}C^C_{31}\right)\widetilde{S}^C_{20} + \left(\frac{3}{5}C^C_{10} - \frac{9}{35}C^C_{30} + \frac{18}{7}C^C_{32}\right)\widetilde{S}^C_{21} + \frac{18}{7}C^S_{32}\widetilde{S}^S_{21} + \left(\frac{6}{5}C^C_{11} - \frac{18}{35}C^C_{31} + \frac{108}{7}C^C_{33}\right)\widetilde{S}^C_{22} + \left(\frac{6}{5}C^S_{11} - \frac{18}{35}C^S_{31} + \frac{108}{7}C^S_{33}\right)\widetilde{S}^S_{22} \quad \text{(C4)}$$

$$\left[C(\Omega)\widetilde{S}(\Omega)\right]^{S}_{11} = C^S_{11}\widetilde{S}^C_{00} + \frac{3}{5}C^S_{21}\widetilde{S}^C_{10} + \frac{6}{5}C^S_{22}\widetilde{S}^C_{11} + \left(C^C_{00} - \frac{1}{5}C^C_{20} - \frac{6}{5}C^C_{22}\right)\widetilde{S}^S_{11} + \left(-\frac{1}{5}C^S_{11} + \frac{18}{35}C^S_{31}\right)\widetilde{S}^C_{20} + \frac{18}{7}C^S_{32}\widetilde{S}^C_{21} + \left(\frac{3}{5}C^C_{10} - \frac{9}{35}C^C_{30} - \frac{18}{7}C^C_{32}\right)\widetilde{S}^S_{21} + \left(-\frac{6}{5}C^S_{11} + \frac{18}{35}C^S_{31} + \frac{108}{7}C^S_{33}\right)\widetilde{S}^C_{22} + \left(\frac{6}{5}C^C_{11} - \frac{18}{35}C^C_{31} - \frac{108}{7}C^C_{33}\right)\widetilde{S}^S_{22} \quad \text{(C5)}$$

Finally, for degree 2 we have

$$\left[C(\Omega)\widetilde{S}(\Omega)\right]^{C}_{20} = C^C_{20}\widetilde{S}^C_{00} + \left(\frac{2}{3}C^C_{10} + \frac{3}{7}C^C_{30}\right)\widetilde{S}^C_{10} + \left(-\frac{1}{3}C^C_{11} + \frac{6}{7}C^C_{31}\right)\widetilde{S}^C_{11} + \left(-\frac{1}{3}C^S_{11} + \frac{6}{7}C^S_{31}\right)\widetilde{S}^S_{11} + \left(C^C_{00} + \frac{2}{7}C^C_{20} + \frac{2}{7}C^C_{40}\right)\widetilde{S}^C_{20} + \left(\frac{3}{7}C^C_{21} + \frac{10}{7}C^C_{41}\right)\widetilde{S}^C_{21} + \left(\frac{3}{7}C^S_{21} + \frac{10}{7}C^S_{41}\right)\widetilde{S}^S_{21} + \left(-\frac{24}{7}C^C_{22} + \frac{60}{7}C^C_{42}\right)\widetilde{S}^C_{22} + \left(-\frac{24}{7}C^S_{22} + \frac{60}{7}C^S_{42}\right)\widetilde{S}^S_{22} \quad \text{(C6)}$$

$$\left[C(\Omega)\widetilde{S}(\Omega)\right]^C_{21} = C^C_{21}\widetilde{S}^C_{00} + \left(\frac{1}{3}C^C_{11} + \frac{4}{7}C^C_{31}\right)\widetilde{S}^C_{10} + \left(\frac{1}{3}C^C_{10} - \frac{1}{7}C^C_{30} + \frac{10}{7}C^C_{32}\right)\widetilde{S}^C_{11} + \frac{10}{7}C^S_{32}\widetilde{S}^S_{11} + \left(\frac{1}{7}C^C_{21} + \frac{10}{21}O^C_{41}\right)\widetilde{S}^C_{20} + \left(C^C_{00} + \frac{1}{7}C^C_{20} - \frac{4}{21}C^C_{40} + \frac{6}{7}C^C_{22} + \frac{20}{7}C^C_{42}\right)\widetilde{S}^C_{21} + \left(\frac{6}{7}C^S_{22} + \frac{20}{7}C^S_{42}\right)\widetilde{S}^S_{21} + \left(\frac{6}{7}C^C_{21} - \frac{10}{21}C^C_{41} + 20C^C_{43}\right)\widetilde{S}^C_{22} + \left(\frac{6}{7}C^S_{21} - \frac{10}{21}C^S_{41} + 20C^S_{43}\right)\widetilde{S}^S_{22} \quad \text{(C7)}$$

$$\left[C(\Omega)\widetilde{S}(\Omega)\right]^S_{21} = C^S_{21}\widetilde{S}^C_{00} + \left(\frac{1}{3}C^S_{11} + \frac{4}{7}C^S_{31}\right)\widetilde{S}^C_{10} + \frac{10}{7}C^S_{32}\widetilde{S}^C_{11} + \left(\frac{1}{3}C^C_{10} - \frac{1}{7}C^C_{30} - \frac{10}{7}C^C_{32}\right)\widetilde{S}^S_{11} + \left(\frac{1}{7}C^S_{21} + \frac{10}{21}C^S_{41}\right)\widetilde{S}^C_{20} + \left(\frac{6}{7}C^S_{22} + \frac{20}{7}C^S_{42}\right)\widetilde{S}^C_{21} + \left(C^C_{00} + \frac{1}{7}C^C_{20} - \frac{4}{21}C^C_{40} - \frac{6}{7}C^C_{22} - \frac{20}{7}C^C_{42}\right)\widetilde{S}^S_{21} + \left(-\frac{6}{7}C^S_{21} + \frac{10}{21}C^S_{41} + 20C^S_{43}\right)\widetilde{S}^C_{22} + \left(\frac{6}{7}C^C_{21} - \frac{10}{21}C^C_{41} - 20C^C_{43}\right)\widetilde{S}^S_{22} \quad \text{(C8)}$$

$$\left[C(\Omega)\widetilde{S}(\Omega)\right]^C_{22} = C^C_{22}\widetilde{S}^C_{00} + \frac{5}{7}C^C_{32}\widetilde{S}^C_{10} + \left(\frac{1}{6}C^C_{11} - \frac{1}{14}C^C_{31} + \frac{15}{7}C^C_{33}\right)\widetilde{S}^C_{11} + \left(-\frac{1}{6}C^S_{11} + \frac{1}{14}C^S_{31} + \frac{15}{7}C^S_{33}\right)\widetilde{S}^S_{11} + \left(-\frac{2}{7}C^C_{22} + \frac{5}{7}C^C_{42}\right)\widetilde{S}^C_{20} + \left(\frac{3}{14}C^C_{21} - \frac{5}{42}C^C_{41} + 5C^C_{43}\right)\widetilde{S}^C_{21} + \left(-\frac{3}{14}C^S_{21} + \frac{5}{42}C^S_{41} + 5C^S_{43}\right)\widetilde{S}^S_{21} + \left(C^C_{00} - \frac{2}{7}C^C_{20} + \frac{1}{21}C^C_{40} + 40C^C_{44}\right)\widetilde{S}^C_{22} + 40C^S_{44}\widetilde{S}^S_{22} \quad \text{(C9)}$$

$$\left[C(\Omega)\widetilde{S}(\Omega)\right]^S_{22} = C^S_{22}\widetilde{S}_{00} + \frac{5}{7}C^S_{32}\widetilde{S}^C_{10} + \left(\frac{1}{6}C^S_{11} - \frac{1}{14}C^S_{31} + \frac{15}{7}C^S_{33}\right)\widetilde{S}^C_{11} + \left(\frac{1}{6}C^C_{11} - \frac{1}{14}C^C_{31} - \frac{15}{7}C^C_{33}\right)\widetilde{S}^S_{11} + \left(-\frac{2}{7}C^S_{22} + \frac{5}{7}C^S_{42}\right)\widetilde{S}^C_{20} + \left(\frac{3}{14}C^S_{21} - \frac{5}{42}C^S_{41} + 5C^S_{43}\right)\widetilde{S}^C_{21} + \left(\frac{3}{14}C^C_{21} - \frac{5}{42}C^C_{41} - 5C^C_{43}\right)\widetilde{S}^S_{21} + 40C^S_{44}\widetilde{S}^C_{22} + \left(C^C_{00} - \frac{2}{7}C^C_{20} + \frac{1}{21}C^C_{40} - 40C^C_{44}\right)\widetilde{S}^S_{22} \quad \text{(C10)}$$

[91] **Acknowledgments.** We thank H.-P. Plag, an anonymous reviewer, and T. Herring for their constructive reviews. We gratefully acknowledge contributions by: T. van Dam, H.-P. Plag, and P. Gegout of the IERS Global Geophysical Fluids Center's "Special Bureau for Loading" for discussions on the need for self-consistent integration of models; G. Balmino for correspondence on Wigner 3-*j* theory and product-to-sum conversion; and D. Lavallée for providing scaled formal errors of the load moment data and for producing Figure 2. This work was supported in the U.S. by the National Science Foundation, Geophysics Program, grant EAR-0125575, and in the U.K. by the Natural Environment Research Council, grant NER/A/S/2001/01166.

References

Agnew, D. C., and W. E. Farrell, Self-consistent equilibrium ocean tides, *Geophys. J. R. Astron. Soc.*, *55*, 171–182, 1978.

Balmino, G., On the product of Legendre functions as encountered in geodynamics, *Stud. Geophys. Geod.*, *22*, 107–118, 1978.

Balmino, G., Gravitational potential harmonics from the shape of an homogeneous body, *Celestial Mech. Dyn. Astron.*, *60*, 331–364, 1994.

Balmino, G., K. Lambeck, and W. M. Kaula, A spherical harmonic analysis of Earth's topography, *J. Geophys. Res.*, *78*, 478–481, 1973.

Blewitt, G., Self-consistency in reference frames, geocenter definition, and surface loading of the solid Earth, *J. Geophys. Res.*, *108*(B2), 2103, doi:10.1029/2002JB002082, 2003.

Blewitt, G., and D. Lavallée, Effect of annual signals on geodetic velocity, *Journ. Geophys. Res.*, *107*(B7), 2145, doi:10.1029/2001JB000570, 2002.

Blewitt, G., D. Lavallée, P. Clarke, and K. Nurutdinov, A new global mode of Earth deformation: Seasonal cycle detected, *Science*, *294*, 2342–2345, 2001.

Chang, A. T. C., J. L. Foster, and D. K. Hall, Satellite estimates of Northern Hemisphere snow volume, *Int. J. Remote Sens.*, *11*, 167–172, 1990.

Chao, B. F., and W. P. O'Connor, Effect of a uniform sea-level change on the Earth's rotation and gravitational field, *Geophys. J.*, *93*, 191–193, 1988.

Chao, B. F., W. P. O'Connor, A. T. C. Chang, D. K. Hall, and J. L. Foster, Snow-load effect on the Earth's rotation and gravitational field, 1979–1985, *J. Geophys. Res.*, *92*, 9415–9422, 1987.

Chen, J. L., C. R. Wilson, D. P. Chambers, R. S. Nerem, and B. D. Tapley, Seasonal global water mass balance and mean sea level variations, *Geophys. Res. Lett.*, *25*, 3555–3558, 1998.

Chen, J. L., C. R. Wilson, B. D. Tapley, D. P. Chambers, and T. Pekker, Hydrological impacts on seasonal sea level change, *Global Planet. Change*, *32*, 25–32, 2002.

Dahlen, F. A., The passive influence of the oceans upon the rotation of the Earth, *Geophys. J. R. Astron. Soc.*, *46*, 363–406, 1976.

Dai, A., and K. E. Trenberth, Estimates of freshwater discharge from continents: Latitudinal and seasonal variations, *J. Hydrometeorol.*, *3*, 660–687, 2002.

Davies, P., and G. Blewitt, Methodology for global geodetic time series estimation: A new tool for geodynamics, *J. Geophys. Res.*, *105*, 11,083–11,100, 2000.

Dickman, S. R., A complete spherical harmonic approach to luni-solar tides, *Geophys. J. Int*, *99*, 457–468, 1989.

Dong, D. J. Dickey, Y. Chao, and M. K. Cheng, Geocenter variations caused by atmosphere, ocean and surface ground water, *Geophys. Res. Lett.*, *24*, 1867–1870, 1997.

Dziewonski, A. M., and D. L. Anderson, Preliminary reference Earth model, *Phys. Earth Planet. Inter.*, *25*, 297–356, 1981.

Farrell, W. E., Deformation of the Earth by surface loads, *Rev. Geophys.*, *10*, 761–797, 1972.

Grafarend, E. W., Three-dimensional deformation analysis: Global vector spherical harmonic and local finite element representation, *Tectonophysics*, *130*, 337–359, 1986.

Grafarend, E. W., J. Engels, and P. Varga, The spacetime gravitational field of a deforming body, *J. Geod.*, *72*, 11–30, 1997.

Heflin, M. B., et al., Global geodesy using GPS without fiducial sites, *Geophys. Res. Lett.*, *19*, 131–134, 1992.

Lambeck, K., *The Earth's Variable Rotation*, Cambridge Univ. Press, New York, 1980.

Lambeck, K., *Geophysical Geodesy: The Slow Deformations of the Earth*, Oxford Univ. Press, New York, 1988.

Lavallée, D., Plate tectonic motions from global GPS measurements, Ph.D. thesis, Univ. of Newcastle, Newcastle upon Tyne, UK, 2000.

Lavallée, D., and G. Blewitt, Degree-1 Earth deformation from very long baseline interferometry, *Geophys. Res. Lett.*, *29*(20), 1967, doi:10.1029/2002GL015883, 2002.

Love, A. E. H., The yielding of the Earth to disturbing forces, *Proc. R. Soc. London, Ser. A*, *82*, 73–88, 1909.

Messiah, A., *Quantum Mechanics*, vol. II, North-Holland, New York, 1963.

Minster, J. F., A. Cazenave, Y. V. Serafini, F. Mercier, M. C. Gennero, and P. Rogel, Annual cycle in mean sea level from TOPEX-Poseidon and ERS-1: Inference on the global hydrological cycle, *Global Planet. Change*, *20*, 57–66, 1999.

Mitrovica, J. X., J. L. Davis, and I. I. Shapiro, A spectral formalism for computing three-dimensional deformations due to surface loads: 1. Theory, *J. Geophys. Res.*, *99*, 7057–7073, 1994.

Munk, W. H., and G. J. F. MacDonald, *The Rotation of the Earth*, Cambridge Univ. Press, New York, 1960.

Nerem, R. S., R. J. Eanes, P. F. Thompson, and J. L. Chen, Observations of annual variations of the Earth's gravitational field using satellite laser ranging and geophysical models, *Geophys. Res. Lett.*, *27*, 1783–1786, 2000.

Particle Data Group, 2002 review of particle physics, *Phys. Rev. D*, *66*, 010001, 2002.

Plag, H.-P., H.-U. Juttner, and V. Rautenberg, On the possibility of global and regional inversion of exogenic deformations for mechanical properties of the Earth's interior, *J. Geodyn.*, *21*, 287–309, 1996.

Proudman, J., The condition that a long-period tide shall follow the equilibrium law, *Geophys. J. R. Astron. Soc.*, *3*, 9423–9430, 1960.

Rikitake, T., R. Sato, and Y. Hagiwara, Applied Mathematics for Earth Scientists, D. Reidel, Norwell, Mass., 1987.

Tamisiea, M. E., J. X. Mitrovica, J. Tromp, and G. A. Milne, Present-day secular variations in the low-degree harmonics of the geopotential: Sensitivity analysis on spherically symmetric Earth models, *J. Geophys. Res.*, *107*(B12), 2378, doi:10.1029/2001JB000696, 2002.

Trenberth, K., Seasonal variations in global sea level pressure and the total mass of the atmosphere, *J. Geophys. Res.*, *86*, 5238–5246, 1981.

van Dam, T. M., J. Wahr, Y. Chao, and E. Leuliette, Predictions of crustal deformation and of geoid and sea-level variability caused by oceanic and atmospheric loading, *Geophys. J. Int.*, *129*, 507–517, 1997.

van Dam, T. M., J. Wahr, P. C. D. Milly, A. B. Shmakin, G. Blewitt, and K. M. Larson, Crustal displacements due to continental water loading, *Geophys. Res. Lett.*, *28*, 651–654, 2001.

Wahr, J. M., The effects of the atmosphere and oceans on the Earth's wobble. 1 Theory, *Geophys. J. R. Astron. Soc.*, *70*, 349–372, 1982.

Wahr, J. M., M. Molenaar, and F. Bryan, Time variability of the Earth's gravity field: Hydrological and oceanic effects and their possible detection using GRACE, *J. Geophys. Res.*, *103*, 30,205–30,229, 1998.

Wigner, E. P., *Group Theory and Its Applications to Quantum Mechanics of Atomic Spectra*, Academic, San Diego, Calif., 1959.

G. Blewitt, Univ. of Nevada, Reno, Mail Stop 178, Reno, NV 89557, USA. (gblewitt@unr.edu)

P. Clarke, School of Civil Engineering and Geosciences, University of Newcastle, Bedson Bldg., Newcastle upon Tyne NE1 7RU, UK. (peter.clarke@ncl.ac.uk)

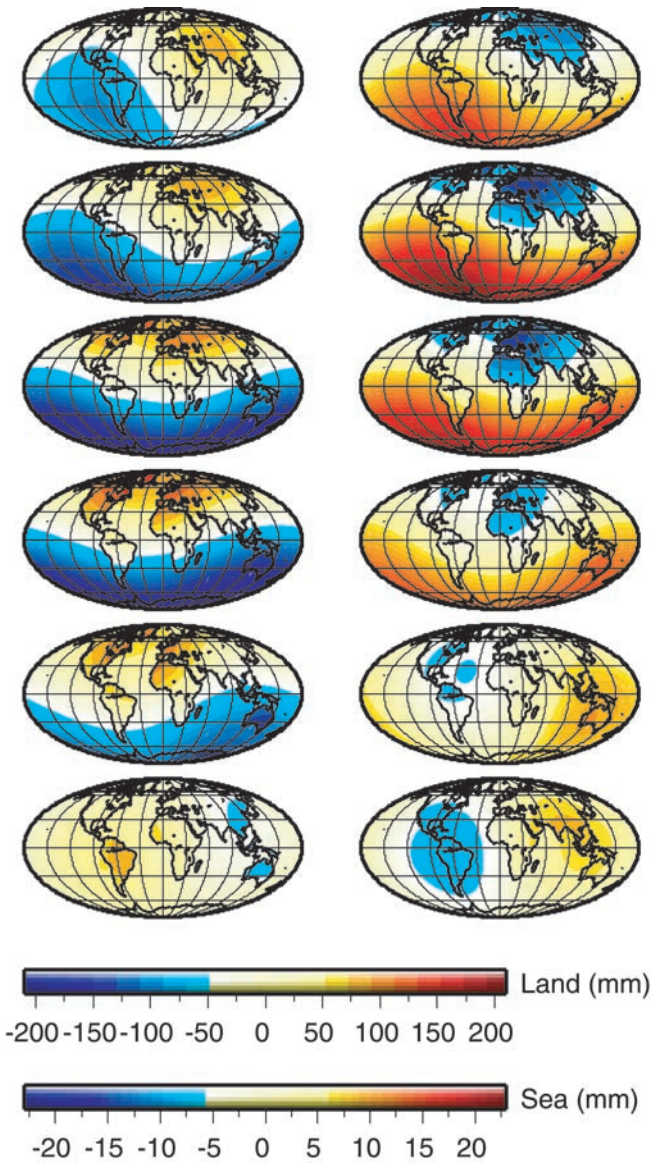

Figure 2. Monthly snapshots of mass distribution on land and in the oceans derived from observed degree-1 deformation: (left) (top to bottom) 1 January through 1 June, and (right) 1 July through 1 December. Different scales are used for land and ocean distributions, as there is a factor of 10 more load variation on land than in the oceans.